

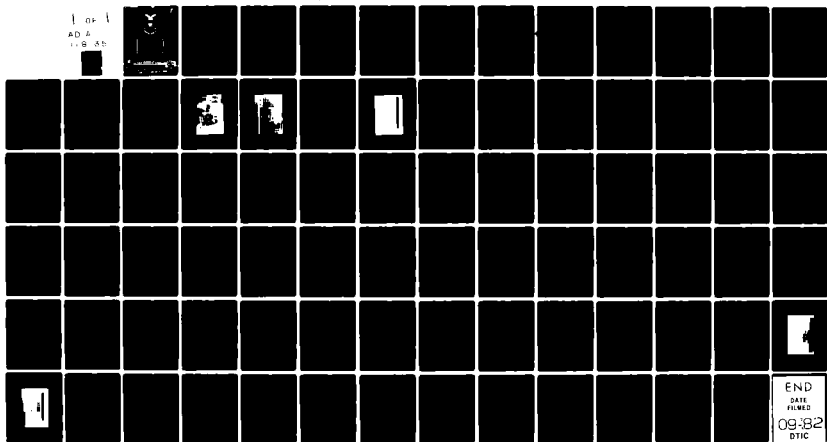
AD-A118 135

AIR FORCE INST OF TECH WRIGHT-PATTERSON AFB OH SCHOO--ETC F/G 21/5  
VISCOELASTIC DAMPING OF TURBINE AND COMPRESSOR BLADE VIBRATIONS--ETC(U)  
MAR 82 S L VEST  
AFIT/GAE/AA/81D-32

UNCLASSIFIED

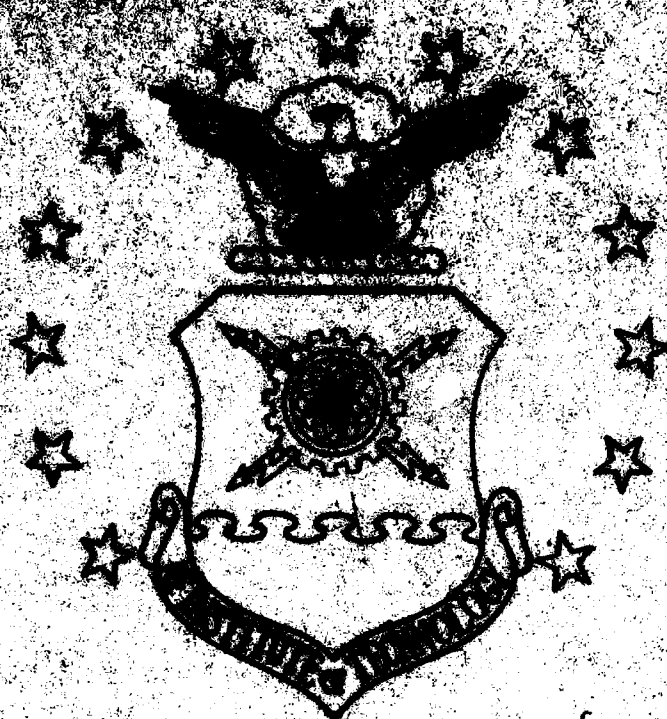
NL

1 of 1  
AD A  
1-8 5b



END  
DATE  
FILMED  
09:82  
DTIC

AD A118135



DEPARTMENT OF THE AIR FORCE  
OFFICE OF THE SECRETARY

AIR FORCE OFFICE OF TECHNOLOGY

DTIC

①

VISCOELASTIC DAMPING OF  
TURBINE AND COMPRESSOR BLADE VIBRATIONS  
THESIS

AFIT/GAE/AA/81D-32 STEPHEN L. <sup>el</sup>VEST  
CAPT USAF

SEP 1 1982

Approved for public release; distribution unlimited

HYDROELASTIC DAMPING OF  
TURBINE AND COMPRESSOR BLADE VIBRATIONS

THESIS

Presented to the Faculty of the School of Engineering  
of the Air Force Institute of Technology  
Air University  
in Partial Fulfillment of the  
Requirements for the Degree of  
Master of Science

by

Stephen L. Vest, B.S.

CAPT

USAF

Graduate Engineering Aeronautics

March 1982



Accession Per	
NTIS GRA&I	X
DTIC TAB	
Unannounced Justification	
By _____	
Distribution/	
Availability Codes	
Dist	Avail and/or Special
A	

Approved for public release; distribution unlimited

## Preface

I would like to express my sincere gratitude to those individuals who assisted me in this effort. First, a special thanks to my thesis advisor, Dr. Peter J. Torvik. Without his technical guidance, understanding, motivation and numerous weekend hours of his time, this task could not have been completed. I am also very grateful to Dr. J.P. Henderson and his staff at the Metals Behavior Branch, Metals and Ceramics Division, of the Air Force Materials Laboratory, for their technical assistance and the various equipment and materials they provided. Also worthy of note was the excellent support provided by the AFIT fabrication shop. Finally, I want to thank my wife and children for their understanding and encouragement.

Stephen L. Vest

## Contents

	<u>Page</u>
Preface . . . . .	ii
List of Figures . . . . .	iv
List of Symbols . . . . .	vi
List of Tables . . . . .	viii
Abstract . . . . .	ix
I Introduction . . . . .	1
II Experimental Development . . . . .	3
Model Description . . . . .	3
Test Set-Up . . . . .	9
Test Procedures . . . . .	12
Data and Discussion . . . . .	14
III Analytical Development . . . . .	33
Model Description . . . . .	33
Viscoelastic Properties . . . . .	33
Boundary Conditions at the Root . . . . .	35
Beam Equation . . . . .	36
Boundary Conditions . . . . .	37
Results . . . . .	42
Analysis of Rigid Body Mode . . . . .	43
IV Sensitivity Analysis and Discussion . . . . .	46
V Conclusion . . . . .	52
Bibliography . . . . .	53
Appendix A: Spring Beam Calibration . . . . .	55
Appendix B: Determination of Shaker Stiffness and Mass . . . . .	59
Appendix C: Iterative Solution to Eigenvalue Problem . . . . .	61
Appendix D: Response Analysis of Rigid Body Mode . . . . .	65
Vita . . . . .	68

## List of Figures

<u>Figure</u>		<u>Page</u>
1	Test Set-Up Diagram . . . . .	4
2	Picture of Test Set-Up . . . . .	5
3	Picture of Test Set-Up (Continued) . . . . .	6
4	Blade Configuration and Dimensions . . . . .	7
5	Picture of Spring Beam Used to Simulate Applied Force . . . . .	8
6	Broadband Frequency Sweep (Frequency versus Force Run 1) . . . . .	18
7	Broadband Frequency Sweep (Frequency versus Force/Frequency Run 1) . . .	19
8	Broadband Frequency Sweep (Frequency versus Force Run 2) . . . . .	20
9	Broadband Frequency Sweep (Frequency versus Force/Frequency Run 2) . . .	21
10	Summary of Broadband Frequency Sweep Data . . .	22
11	Narrowband Frequency Sweep for Displacement = 50 $\mu$ inches (Frequency versus Force Run 1) . . . . .	23
12	Narrowband Frequency Sweep For Displacement = 50 $\mu$ inches (Frequency versus Force / Frequency Run 1) . . .	24
13	Narrowband Frequency Sweep For Displacement = 150 $\mu$ inches (Frequency versus Force Run 1) . . . . .	25
14	Narrowband Frequency Sweep For Displacement = 150 $\mu$ inches (Frequency versus Force/Frequency Run 1) . . .	26
15	Narrowband Frequency Sweep For Displacement = 50 $\mu$ inches (Frequency versus Force Run 2) . . . . .	27

<u>Figure</u>		<u>Page</u>
16	Narrowband Frequency Sweep For Displacement = 50 $\mu$ inches (Frequency versus Force/Frequency Run 2) . . .	28
17	Narrowband Frequency Sweep For Displacement = 150 $\mu$ inches (Frequency versus Force Run 2) . . . . .	29
18	Narrowband Frequency Sweep For Displacement = 150 $\mu$ inches (Frequency versus Force/Frequency Run 2) . . .	30
19	Narrowband Frequency Sweep Using Friction Damping For Displacement = 100 $\mu$ inches (Frequency versus Force) . . . . .	31
20	Narrowband Frequency Sweep Using Friction Damping For Displacement = 100 $\mu$ inches (Frequency versus Force/Frequency) . . . . .	32
21	Stiffness and Damping versus Frequency . . . . .	34
22	Modified Cantilever Beam and Sign Convention . . . . .	38
23	Tip Mass versus Frequency (Second Resonant Frequency) . . . . .	47
24	Tip Mass versus Frequency (First Resonant Frequency) . . . . .	48
25	Magnitude of Modulus/Thickness versus Frequency (For Second Resonant Frequency) . . . . .	50
26	Magnitude of Modulus/Thickness versus Frequency (For Third Resonant Frequency) . . .	51
27	Strain Gauge Calibration Curve . . . . .	56
28	Picture of Force Table Used to Calibrate Strain Gauges . . . . .	57
29	Picture of Force Table in Blade Mount . . . .	58
30	Analytical Prediction of Force versus Frequency for Rigid Body Mode at 150 $\mu$ inches Displacement . . . . .	67



### List of Symbols

E	Modulus of elasticity of the blade ( $\text{lb/in}^2$ )
f	Frequency, cycles per second
G	Complex modulus of elastomer ( $\text{lb/in}^2$ )
$G_1$	Real part of complex modulus of elastomer ( $\text{lb/in}^2$ )
$G_2$	Imaginary part of complex modulus of elastomer ( $\text{lb/in}^2$ )
I	Area moment of inertia of the blade ( $\text{in}^4$ )
$I_0$	Mass moment of inertia $\text{lb-sec}^2\text{-in}$
$k_s$	Stiffness of the shaker ( $\text{lb/in}$ )
L	Length of the blade (in)
M	Moment at blade root ( $\text{in-lb}$ )
$M_b$	Mass per unit length of blade ( $\text{lb-sec}^2/\text{in}^2$ )
$M_s$	Mass of shaker and connecting bolt ( $\text{lb-sec}^2/\text{in}$ )
$M_s'$	Mass of shaker, connecting bolt, accelerometer ( $\text{lb-sec}^2/\text{in}$ )
$M_{e,g}$	Mass of linkage, force gauge, accelerometer ( $\text{lb-sec}^2/\text{in}$ )
$M_t$	Tip mass with part of linkage and force gauge, and accelerometer ( $\text{lb-sec}^2/\text{in}$ )
P	Force applied by setscrew and spring beam (lb)
t	Thickness of elastomer (in)
W	Width of blade (in)
$y(x,t)$	Displacement of blade in y direction
$\alpha$	Angle of elastomer contact surface
$\beta$	Eigenvalue
$\epsilon$	Strain

$n$	Loss factor; ratio of $G_1/G_2$
$\omega$	Frequency of vibration (rad/sec)
$\theta_1$	1/2 angle of blade mount cut-out
$\theta_2$	Angle between horizontal and lower edge of elastomer contact surface
$\phi$	Slope of beam ( $\frac{\partial y}{\partial x}$ )
$\sigma$	Stress (lb/in <sup>2</sup> )
$\tau$	Shear stress (lb/in <sup>2</sup> ) in viscoelastic layer
$\mu$	10 <sup>-6</sup>

NOTE: Computer program in Appendix C restates some of the above symbols.

List of Tables

<u>Table</u>		<u>Page</u>
1	ISD 112 Material Properties . . . . .	10
2	Blade and Dovetail Properties . . . . .	11

## ABSTRACT

An experimental and an analytical model of a turbine/compressor blade is developed in order to investigate the feasibility of using a viscoelastic material to dampen the vibrations of the blade. The experimentally determined response of the blade at various frequencies is studied. In order to make a qualitative comparison of damping effectiveness, the response of a similar model using friction damping is also experimentally studied. A model of a modified cantilever beam is used to develop the equation of motion of the blade and the resulting eigenvalue problem is solved using an iterative technique. An analysis of the rigid body mode is performed. A comparison and an analysis of the results of the experimental and analytical models are delineated.

# VISCOELASTIC DAMPING OF VIBRATORY STRESS IN AIRCRAFT STRUCTURES

## I. Introduction

Vibratory energy can cause catastrophic failures in nearly any type of structure. Aircraft structures are certainly no exception, and the problem of how to dissipate this energy has long been an important consideration in their design. In this application, limiting the amplitude of vibrations by stiffening moving parts is normally not the optimum solution since this usually adds to the mass of the system. With greater demands to increase performance, lower thrust to weight ratios can not be tolerated as a primary means of controlling amplitudes of vibrations in aircraft structures.

Problems in aircraft propulsion systems are further exacerbated by the hostile environment. The compressor and turbine blades generate extremely high centrifugal stresses. The turbine blades, in addition, must operate at temperatures ranging from 1500°F to 1900°F with accompanying thermal gradient stresses.

The purpose of the study was to explore the concept of introducing a viscoelastic material at the root of a turbine/compressor blade as a means of damping vibratory oscillations. The avenues to this exploration were an experimental and an analytical model of the blade along with a comparison and analysis of these models.

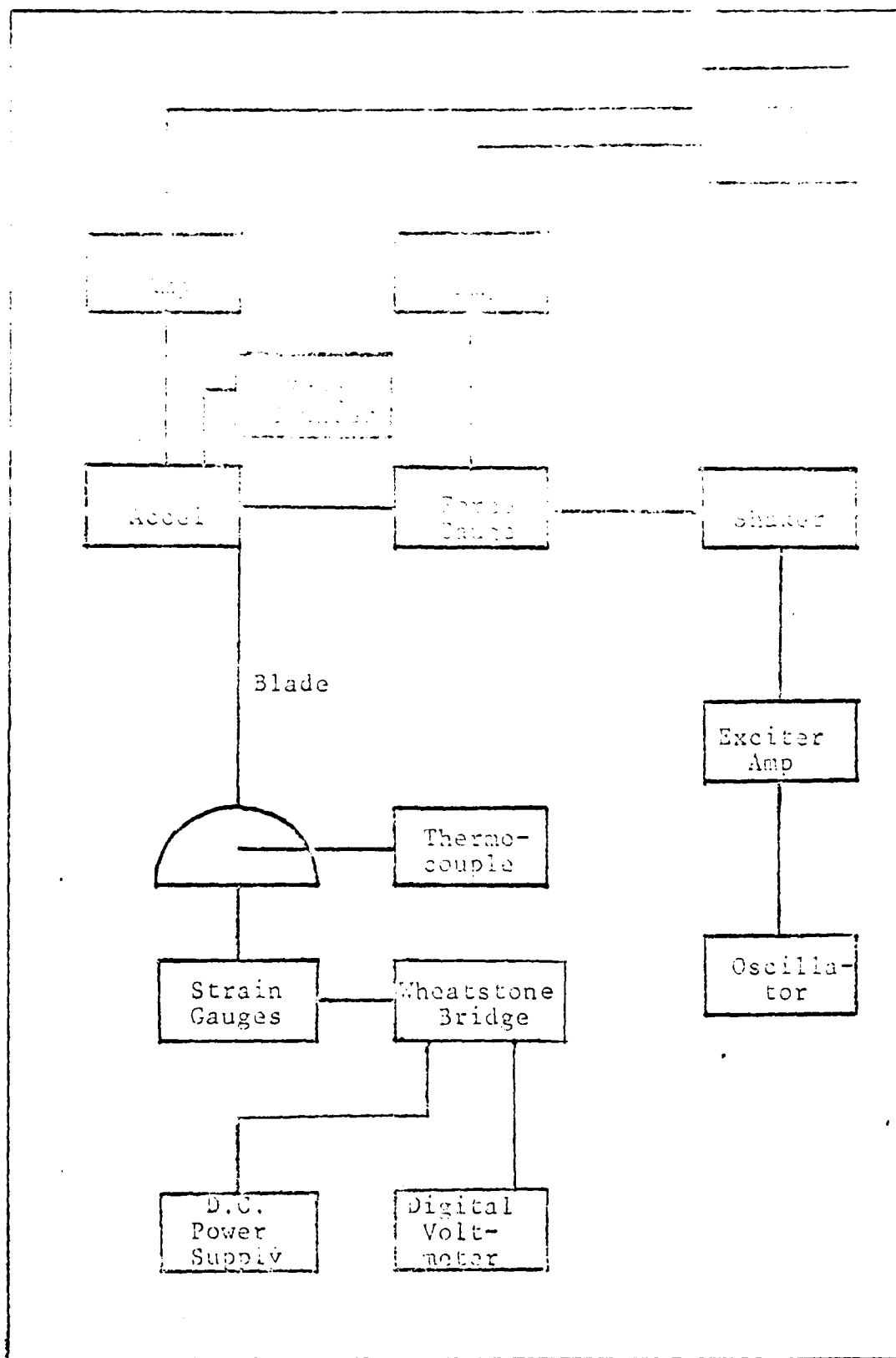
The derivation of an equation of motion satisfying particular boundary conditions was the main objective of the analytical section. The turbine/compressor blade was modeled as a modified cantilever beam with a torsional spring and viscous damper at the root to represent the damping material, and a tip mass with some added stiffness at the tip to account for the shaker stiffness and the mass of the shaker, force gauge, linkage and accelerometer. The solution of the resulting eigenvalue problem was used to predict the resonant frequencies of the blade.

The experimental model was used to compare results measured in the laboratory to those predicted analytically. The frequency of vibration was the parameter that was varied during the tests while monitoring damping layer temperature and thickness, vibration amplitudes and forces, and clamping pressures at the base of the blade.

The preliminary study was conducted at room temperature using a commercially available damping material. Each viscoelastic material has certain frequency and temperature ranges where losses reach a maximum. Consequently, a certain material can be chosen to fit a particular application. If viscoelastic damping at the blade root proves feasible, further studies employing materials usable at engine operating temperatures should be pursued. It is already well known that vitreous materials have high loss factors that can be employed to considerably reduce resonant vibratory energy (Ref 1). Such materials may be desirable in this application.

1. The first step is to identify the problem or question that needs to be answered. This involves understanding the context and the specific requirements of the task.

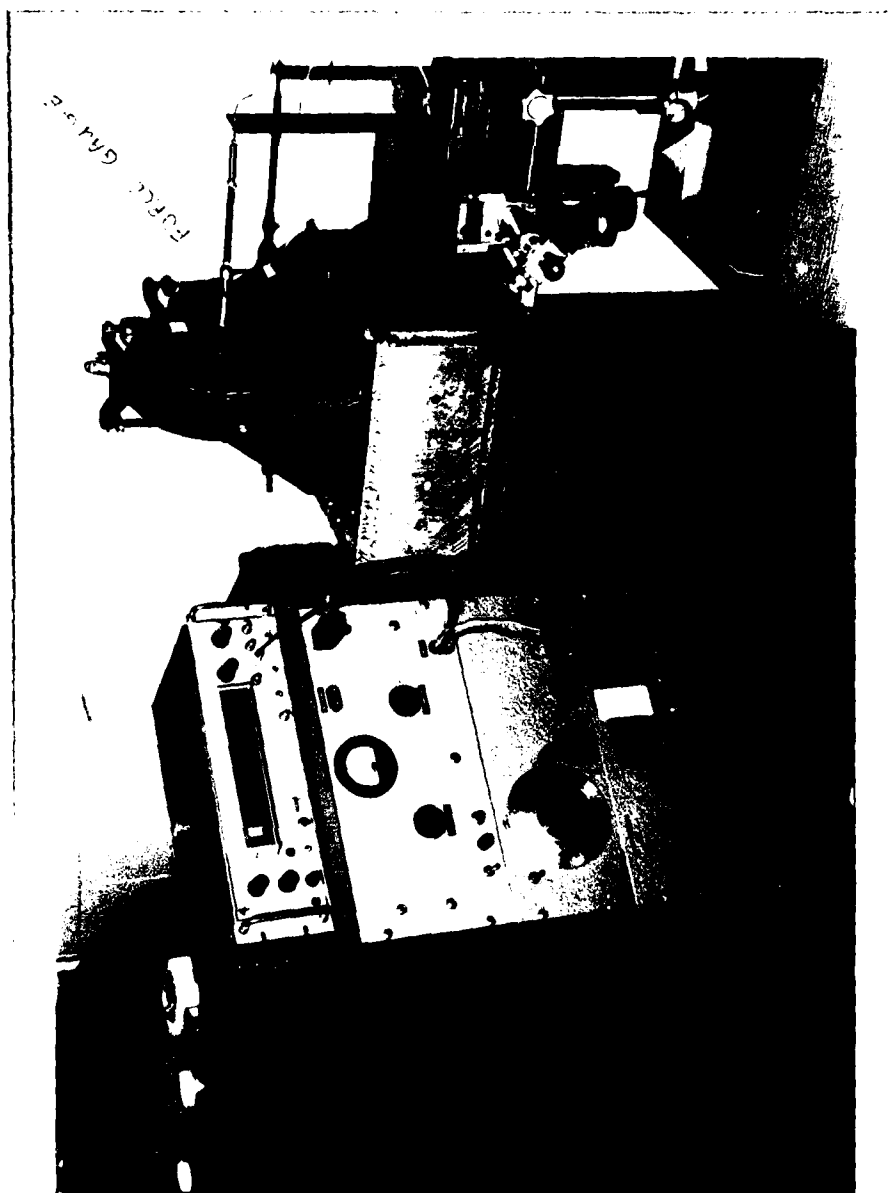
The viscoelastic material used in the experiment was ISD 112. It was chosen because it has peak damping properties at ambient temperatures and at frequencies between  $10^2$  and  $10^3$  cycles per second which were the test conditions.



TEST SET-UP DIAGRAM

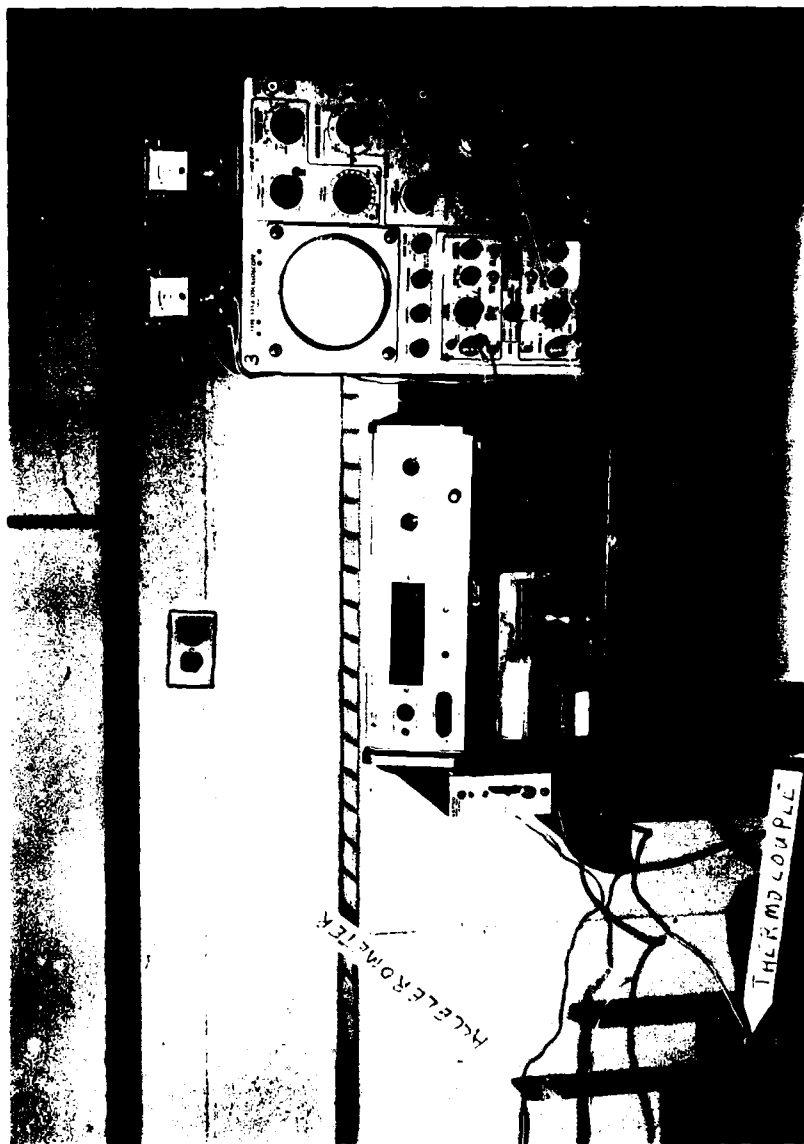
FIGURE 1





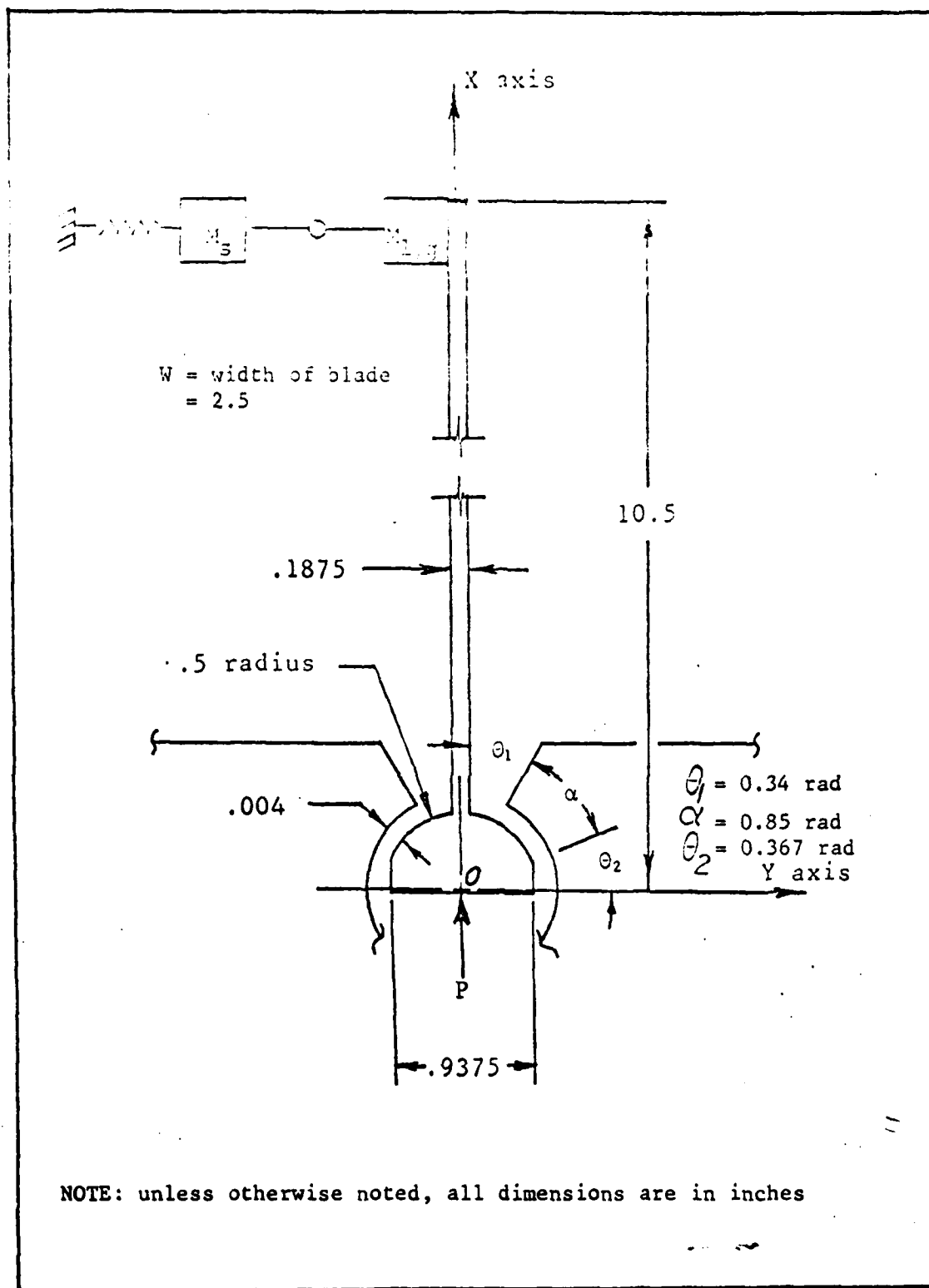
PICTURE OF THE SET UP

FIGURE 2



PICTURE OF TEST SET UP (CONTINUED)

FIGURE 3



BLADE CONFIGURATION AND DIMENSIONS

FIGURE 4



Table 1, an extract from reference 8, lists the actual properties of the material used in the tests.

Table 2 delineates the properties of the blade and the dovetail root.

The mass and stiffness of the shaker were determined experimentally as delineated in Appendix B.

#### Test Set-Up

A schematic diagram of the test set-up is shown in Figure 1. The shaker exciter was a MB Vibration test equipment model T122133. This was used to vary the frequency and amplitude of the sinusoidal signal from the shaker. The frequency was monitored using a Computer Measurements frequency counter, model 726C. The shaker, an MB model 50, was used to simulate a sinusoidal tip loading that would represent the periodic force on a turbine/compressor blade. A PCB force transducer model 208A03 serial number 1934 was mounted in series with the vibrator linkage. For this device, the vendor supplied the calibration factor of 11.6 millivolts per pound. The transducer output (see figures 2 and 4) was then amplified by the variable gain PCB amplifier model 480C06 power unit. The accelerometer (see figures 3 and 4) was a PCB model 303A serial number 2066 with a calibration factor of 14.3 millivolts per g that was also supplied by the vendor. It too was amplified by a similar PCB power unit. Both the force gauge and the accelerometer outputs were measured using a Tektronix oscilloscope model 535A. The copper constantan thermocouple was spot welded to the blade mount in the vicinity of the elastomer

# 100 111 MATERIAL PROPERTIES

<u>MODULUS</u> <u>(N/M<sup>2</sup>)</u>	<u>MODULUS</u> <u>(lb/in<sup>2</sup>)</u>	<u>LOSS</u> <u>FACTOR (%)</u>	<u>TEMP</u> <u>(°C)</u>	<u>FREQ</u> <u>(CPS)</u>
1.147 E+07	1645	.6758	-5.6	469.7
2.037 E+07	2922	.4399	-5.6	1223.2
1.732 E+06	636	.0490	1.4	126.3
3.302 E+06	1262	.3056	1.4	1092.9
1.686 E+06	242	1.0755	18.3	352.4
2.973 E+06	426	1.0867	18.3	894.3
9.622 E+05	138	1.1203	24.4	315.1
1.494 E+06	214	1.1685	24.4	797.4
1.939 E+06	279	1.3745	24.4	1488.4
8.182 E+05	117	1.0131	29.4	304.4
1.328 E+06	190	1.0873	29.4	782.1
1.809 E+06	259	1.1978	29.4	1471.1
5.454 E+05	78	.8981	37.8	284.3
7.361 E+05	106	1.1351	37.8	733.9

TABLE 1

# BLADE AND DOVETAIL PROPERTIES

Blade and Dovetail Material	Inconel-X
Modulus of Elasticity	$31(10^6)$ lb/in <sup>2</sup>
Blade area Moment of Inertia	0.001373 in <sup>4</sup>
Blade Mass	0.003905 lb-sec <sup>2</sup> -in
Dovetail Mass	0.000719 lb-sec <sup>2</sup> -in
Total Mass	0.004624 lb-sec <sup>2</sup> -in
Blade Mass Moment of Inertia	
about point O (see figure 4)	0.1402 lb-sec <sup>2</sup> -in
Dovetail Mass Moment of Inertia	
about point O	0.00001975 lb-sec <sup>2</sup> -in
Total Mass Moment of Inertia	
about point O	0.14021975 lb-sec <sup>2</sup> -in

TABLE 2

for the purpose of measuring the approximate elastomer temperature. The thermocouple was connected to an Omega Engineering digital temperature indicator model 117.

The output from the two IEA strain gauges  $35 \pm 3$  ohms,  $2.01 \times 10^{-3}$  gage factor, type J-11 was measured with a Hewlett-Packard digital voltmeter model 34-0A. The 10 volt potential for the Wheatstone bridge was provided by a Kepco power unit model KB15-0.2. The thickness of the viscoelastic material was measured using a Gaertner microscope serial number 1211X (no model number listed), with a magnification factor of 30.

#### Test Procedure

For each frequency sweep, the displacement at the tip of the blade was held constant by setting the appropriate acceleration as determined in step 5. The strain gauges on the spring beam were calibrated as outlined in Appendix A. Data were collected for these displacements using the following procedure:

1. The elastomer was placed on the blade root.
2. The blade was then aligned inside the blade mount and raised into place using the set screw on the spring beam. The set screw was adjusted to give the proper thickness as monitored on the microscope. When this thickness was obtained, the strain gauge voltage measurements were recorded and from this, the contacting force was determined and the contacting pressure was calculated. The accelerometer and the shaker linkage were then connected to the blade tip.

3. The temperature at the blade root was recorded using



the thermocouple and the temperature display.

4. The first displacement for a data run was chosen. In order to insure that the no slip condition at the elastomer contact surfaces was upheld, a relatively small maximum allowable shearing value of .1 was chosen. For example, for an elastomer thickness of .002 inches, the maximum allowable tip displacement was calculated to be .004 inches. For this thickness the maximum tip displacement used in the test was only .00015 inches, corresponding to a strain of less than .007.

5. The needed acceleration was calculated using:

$$\text{Displacement } (2\pi \times f)^2 = \text{Acceleration}$$

6. Using the oscillator amplitude control on the exciter, the desired acceleration was set as monitored on the oscilloscope.

7. The amplitude of the force was also recorded from the oscilloscope.

8. The frequency was incremented and steps five through seven were repeated for various bands, displacements, and intervals as follows:

- a. 25-100 cps, 150u in, 25 cps intervals
- b. 125-500 cps, 50u in, 25 cps intervals
- c. 725-1000 cps, 10u in, 25 cps intervals
- d. 205-215 cps, 50u in, 5 cps intervals
- e. 215-217 cps, 150u in, 5 cps intervals

In addition, in order to compare the effectiveness of viscoelastic damping with friction damping a frequency sweep

using a slightly different blade model was performed. The model and the technique were developed in a previous AFIT thesis by Capt Michael Kimberling (Ref 13). This modified blade had a dovetail root of one inch diameter and it did not have the 1/32 inch clearances on each side. Essentially, since there was no viscoelastic material sandwiched between the blade root and the mount, the root fit snugly into the mount and the damping present was due to friction. A frequency sweep between 240 cps and 360 cps was performed in increments of ten cps. The amplitude of vibrations was set to 100μ inches and the clamping force was five pounds.

#### Data and Discussion

The data that were collected are presented as plots of frequency of vibrations versus force required to keep the amplitude of vibrations constant. The frequency versus force divided by frequency is also plotted for reasons given below. In theory, as a system approaches vibrations near a resonant frequency, the force required to maintain a constant amplitude approaches zero. In actuality, of course, all physical systems possess some damping; therefore, the force only drops to some minimum value at resonance.

Two important phenomena are important to discern in these plots. The first, as just mentioned, is the decrease in force at resonant frequencies. On the plots of frequency versus force, these points are easily recognized.

The second phenomenon to observe is the flatness of the response over a given bandwidth near a resonant frequency.

This gives a relative measure of the effective mechanical reaction to deformation. In other words, the plotted quantity is proportional to the mechanical impedance of the system. In this report, plots of frequency versus force divided by frequency may be a more effective method of presenting this data. This quantity, at fixed amplitudes of displacement, is proportional to the mechanical impedance of the system.

Figures 4 through 9 are the broadband frequency sweeps at constant values of the displacements, as labeled on the figures. The purpose of this coarse sweep was to identify probable resonant frequencies in a relatively large range of frequencies. Two data runs were performed using different elastomer samples. Analytical predictions of the resonant frequencies are discussed in section III. Values for the first three resonant frequencies were found to be 26.25 cps, 258.3 cps, and 764.9 cps respectively. The first analytically predicted resonance was not discernible even with smaller frequency increments of 5 cps in this range. For both data runs, there was an apparent second resonant frequency at approximately 255-260 cps. The third resonant frequency was measured at 775 cps and 850 cps. The reproducibility of the data for each data run was quite good for the second resonant frequency and only fair for the third resonant frequency. Figure 10 summarizes these broadband sweeps plotted on a logarithmic frequency scale and a logarithmic scale of Force divided by frequency times displacement.

The region near the second resonant frequency of 255-260

cps was chosen to investigate in greater detail by performing frequency sweeps with increments of 5 cps.

Figures 11, 13, 15 and 17 display the characteristic dip in force at resonant frequencies of 255-260 cps for displacements of 50 $\mu$  inches and 150 $\mu$  inches. Furthermore, figures 12, 14, 16 and 18 show the relative flatness of these responses at resonances for the same displacements.

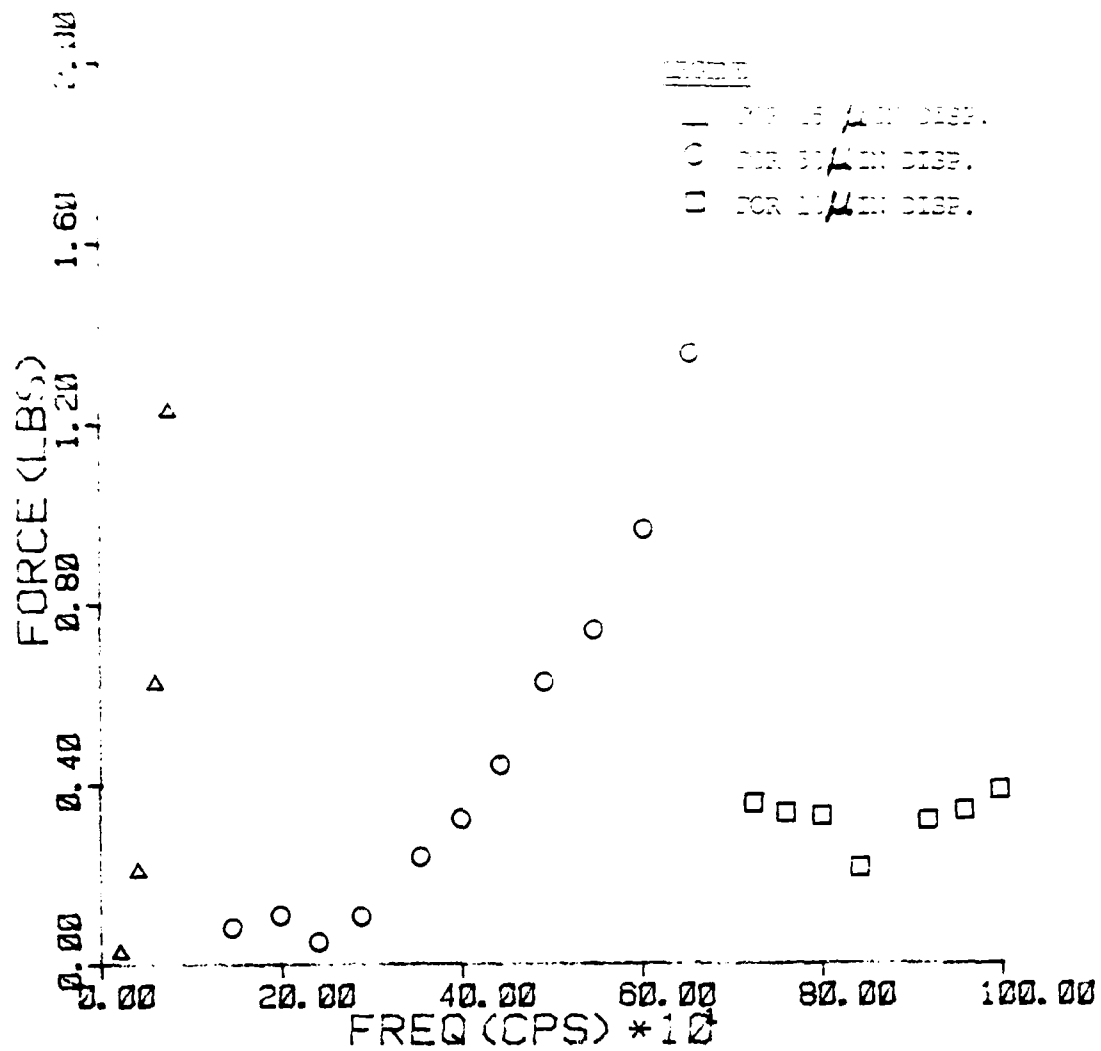
In addition, figures 19 and 20 are plots of responses using friction damping obtained at frequency increments of ten cps. These plots are presented in order to make a qualitative comparison of viscoelastic damping to friction damping. By comparing figures 11 through 18 with figures 19 and 20, the viscoelastically damped responses are shown to be somewhat flatter than the friction damped response, indicating that the elastomer is a more effective damping mechanism. The friction damped system had a resonance at 276 cps and the resonant frequency of the viscoelastic system was 258 cps. The higher resonant frequency for the friction case is not surprising since this is a stiffer system than the one with the elastomer sandwiched in at the blade root.

The following is a list of other pertinent data that were collected during each data run:

	Run 1	Run 2
Average elastomer thickness	.00414 inches	.0050 inches
Temperature of blade root	77°F	76°F
Contact force at blade root	7.2 lbs	4 lbs
Contact pressure at blade root	1.8 lbs/in <sup>2</sup>	1 lb/in <sup>2</sup>

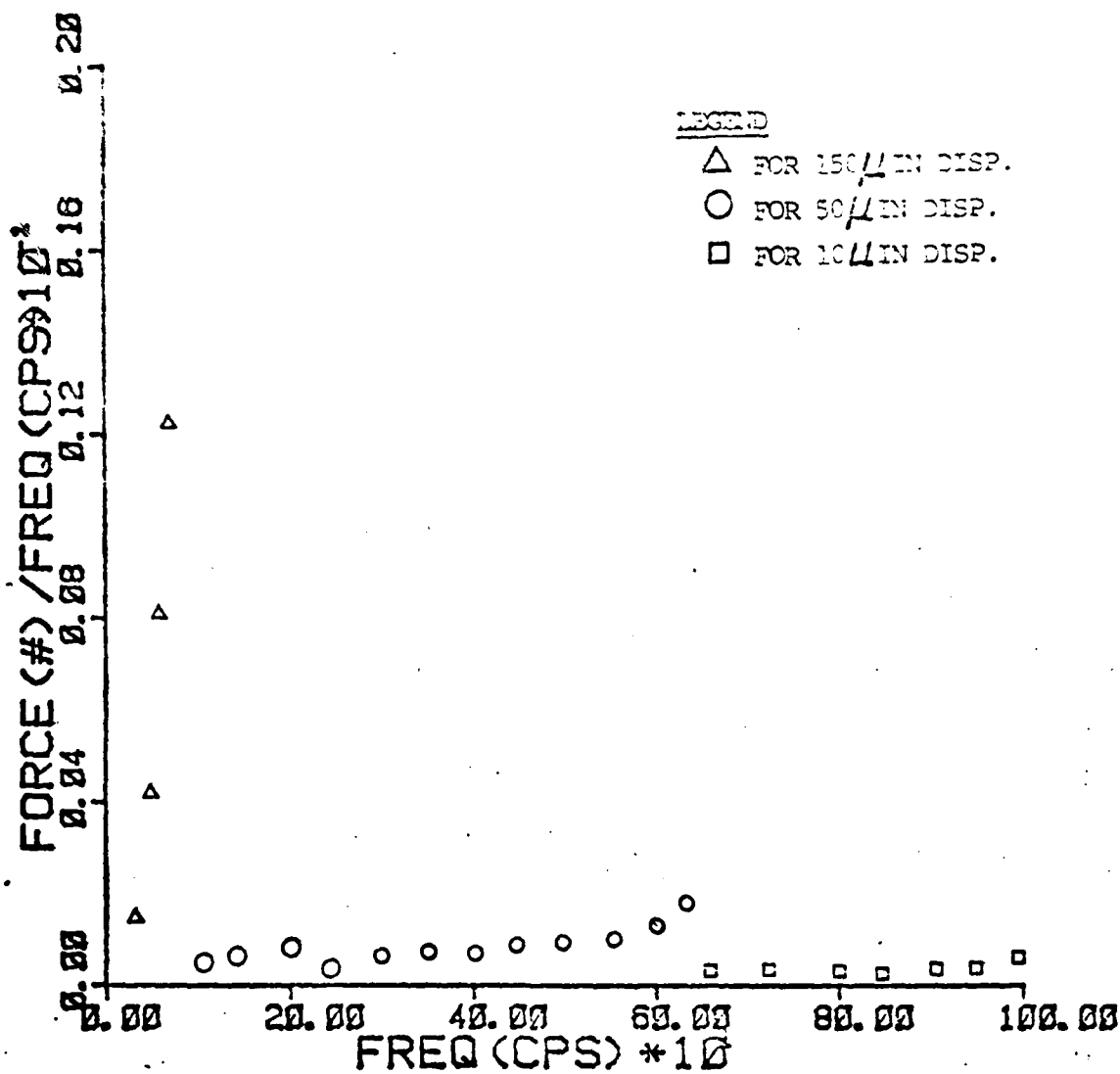
The area used to calculate the above contact pressure was determined using the arc length of the dovetail minus the

about 100 times the width of the blade. The small rotational displacements that alter the overall contact length are negligible.



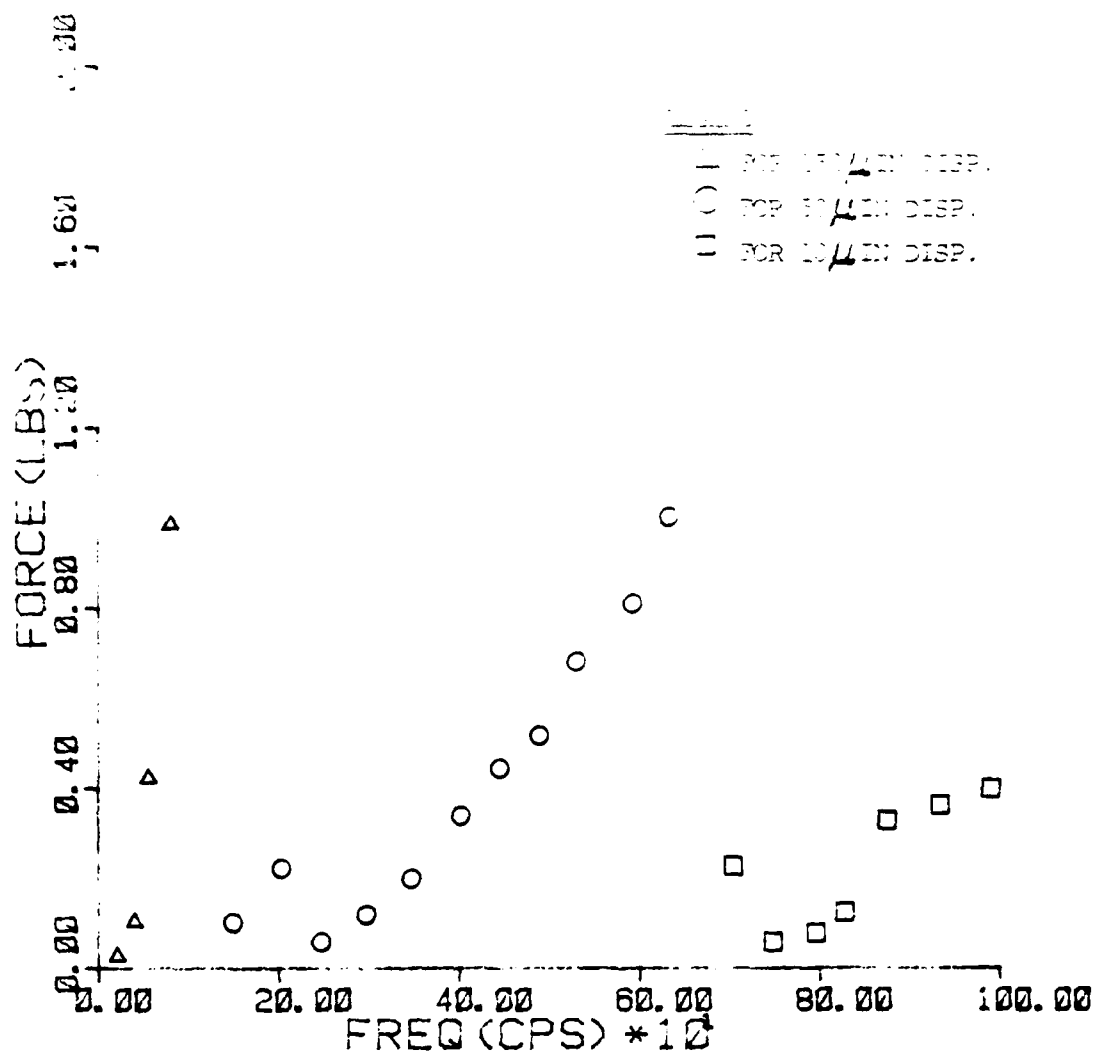
BROADBAND FREQUENCY SWEEP  
 (FREQUENCY VERSUS FORCE RUN 1)

FIGURE 6



BROADBAND FREQUENCY SWEEP  
(FREQUENCY VERSUS FORCE/FREQUENCY RUN1)

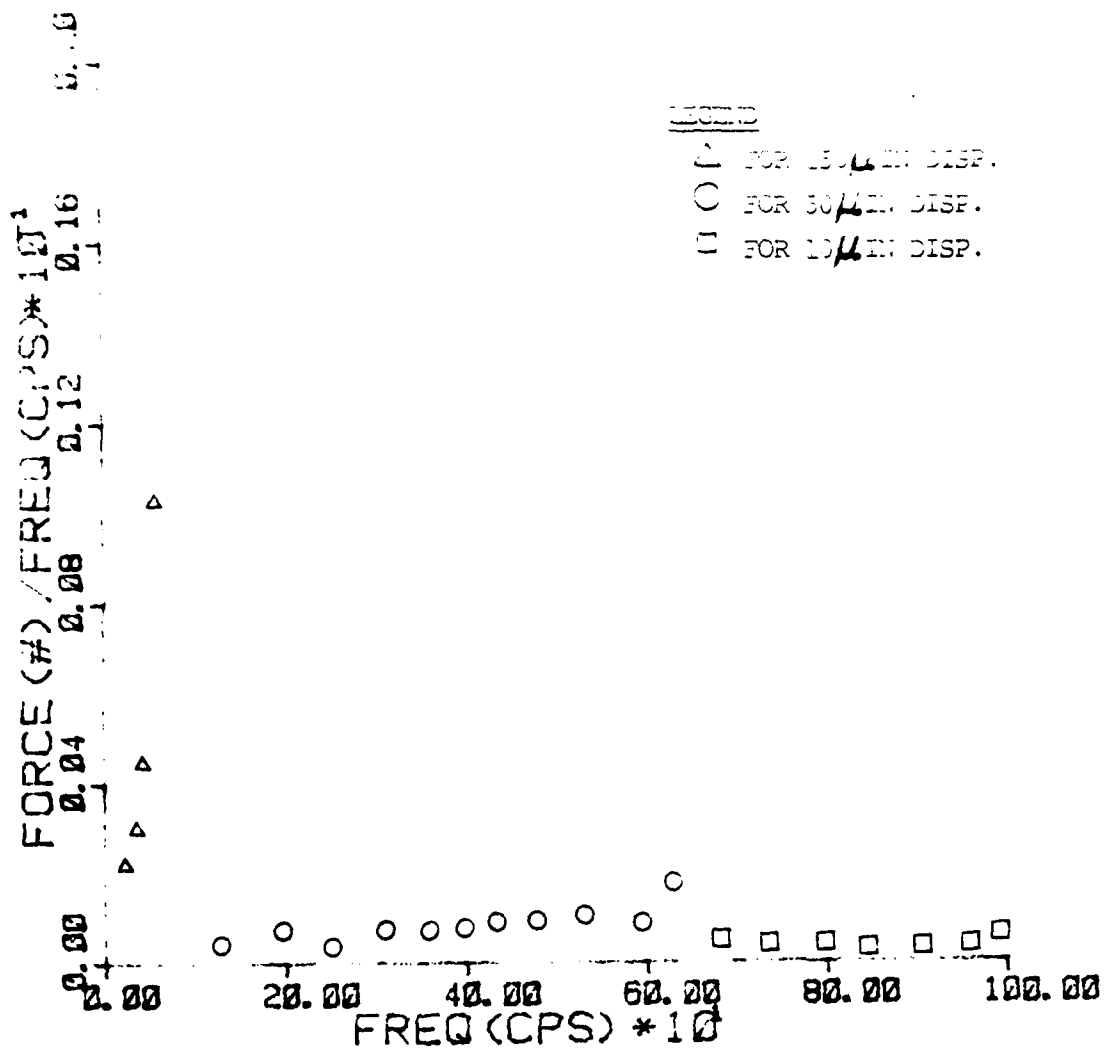
FIGURE 7



BROADBAND FREQUENCY SWEEP  
(FREQUENCY VERSUS FORCE RUN 2)

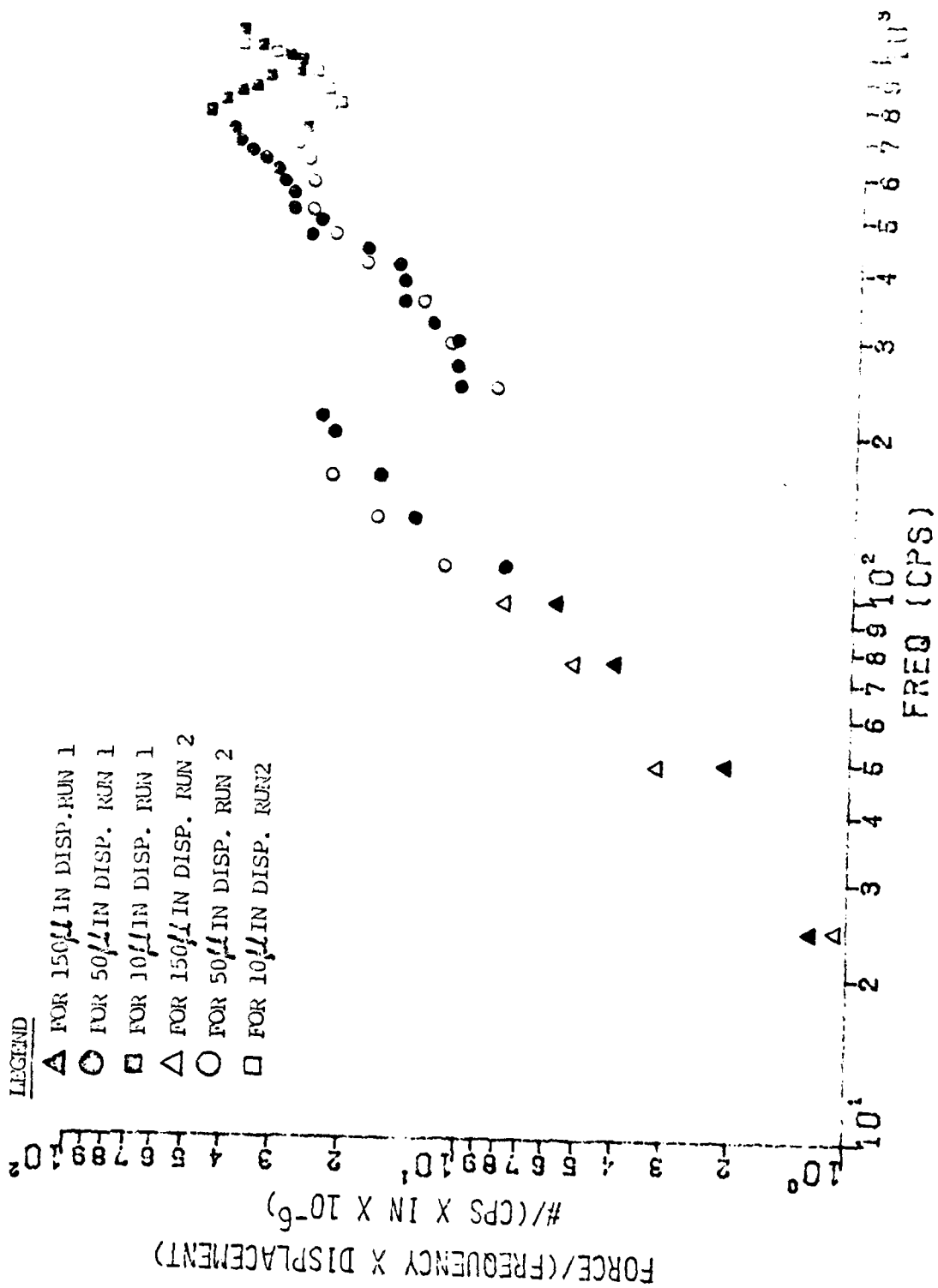
FIGURE 8





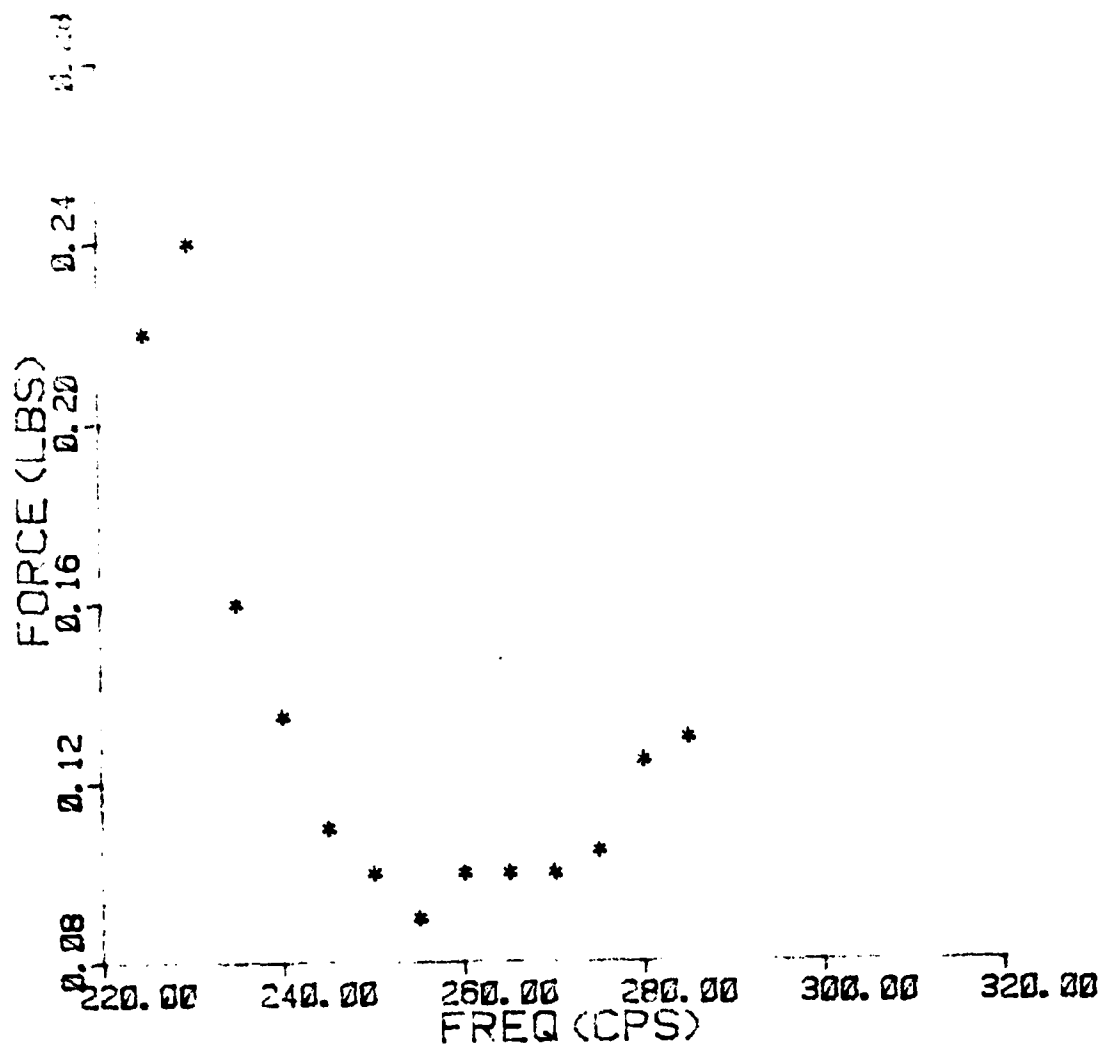
BROADBAND FREQUENCY SWEEP  
(FREQUENCY VERSUS FORCE/FREQUENCY RUN 2)

FIGURE 9



SUMMARY OF BROADBAND FREQUENCY SWEEP DATA

FIGURE 10

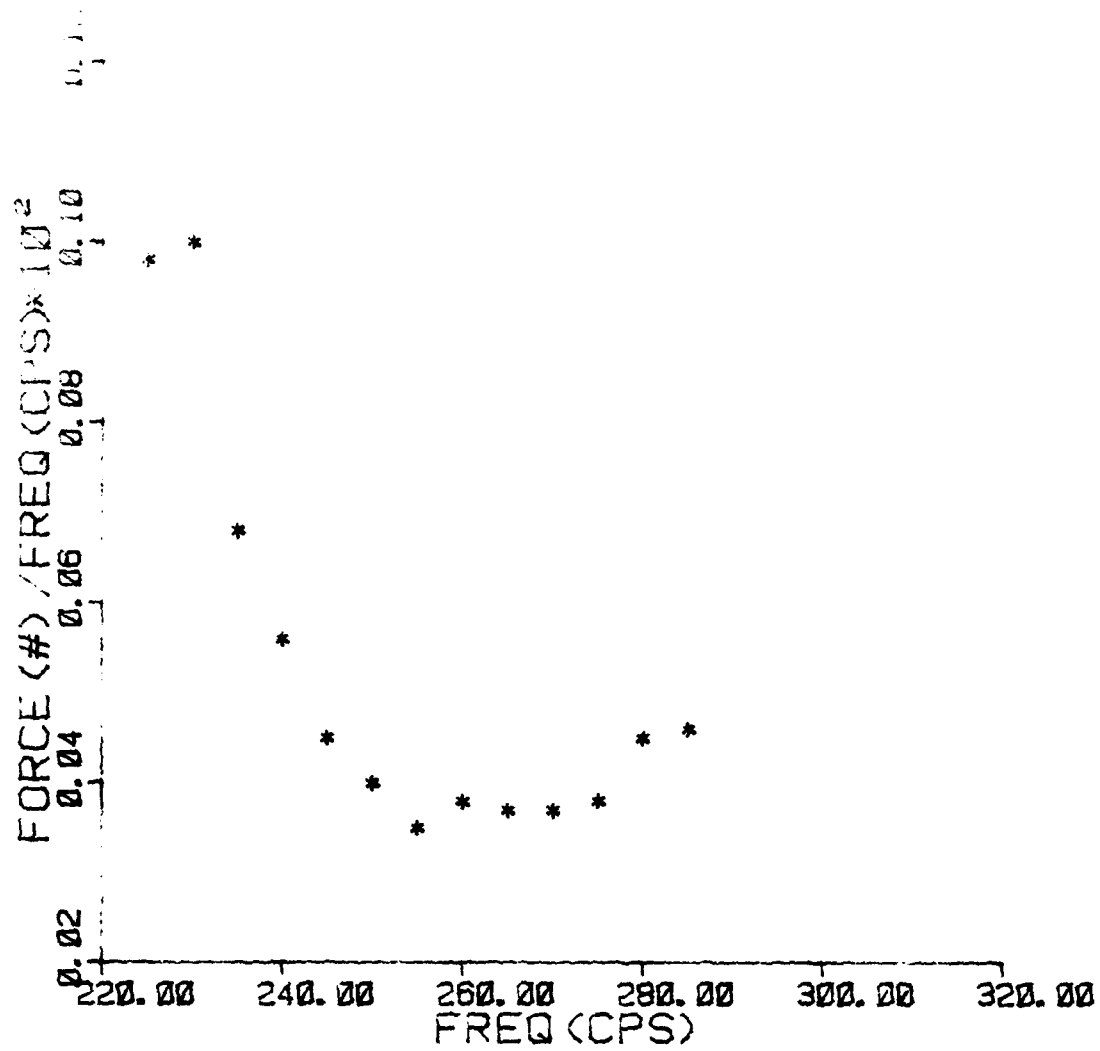


NARROWBAND FREQUENCY SWEEP FOR

DISPLACEMENT = 50  $\mu$  inches

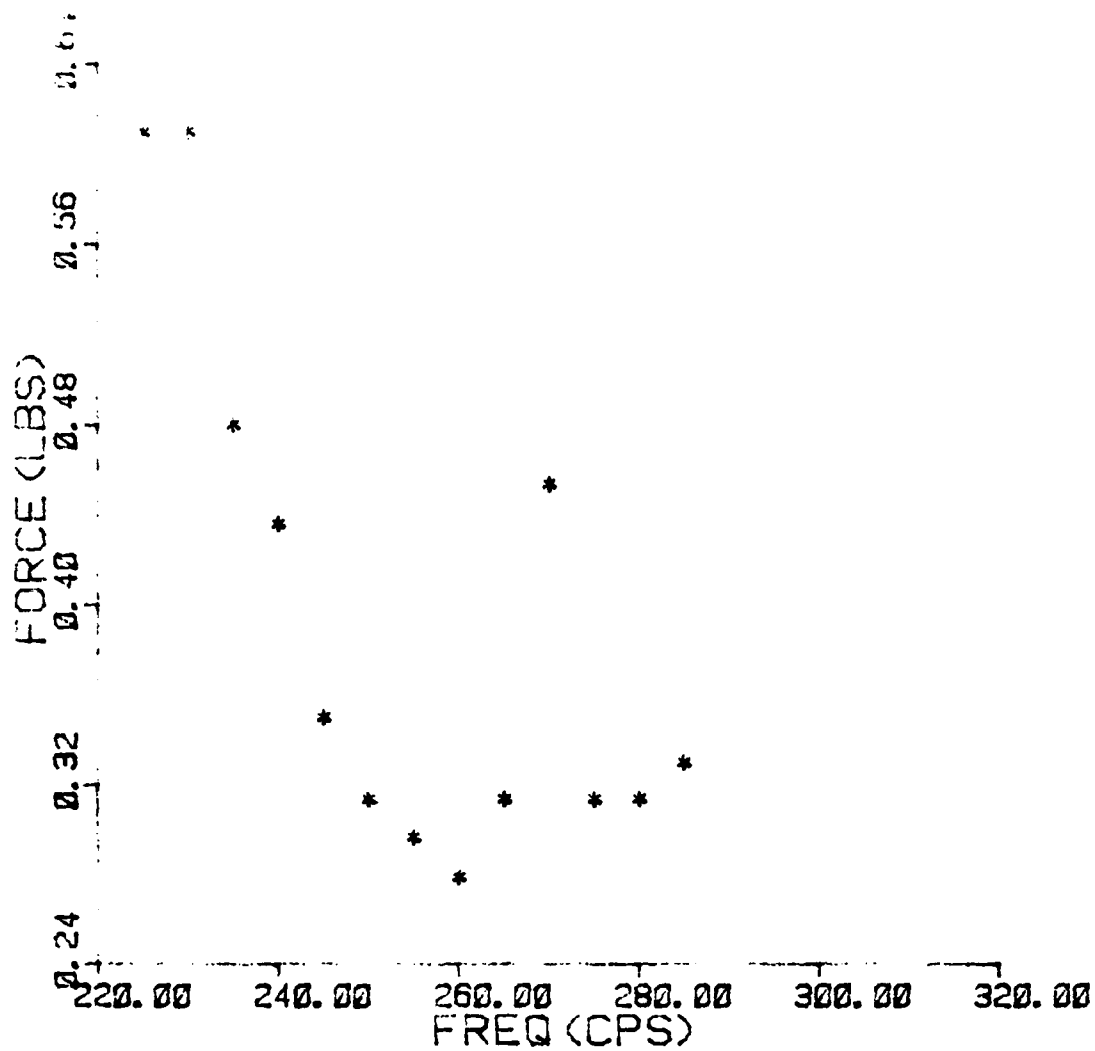
(FREQUENCY VERSUS FORCE RUN1)

FIGURE 11



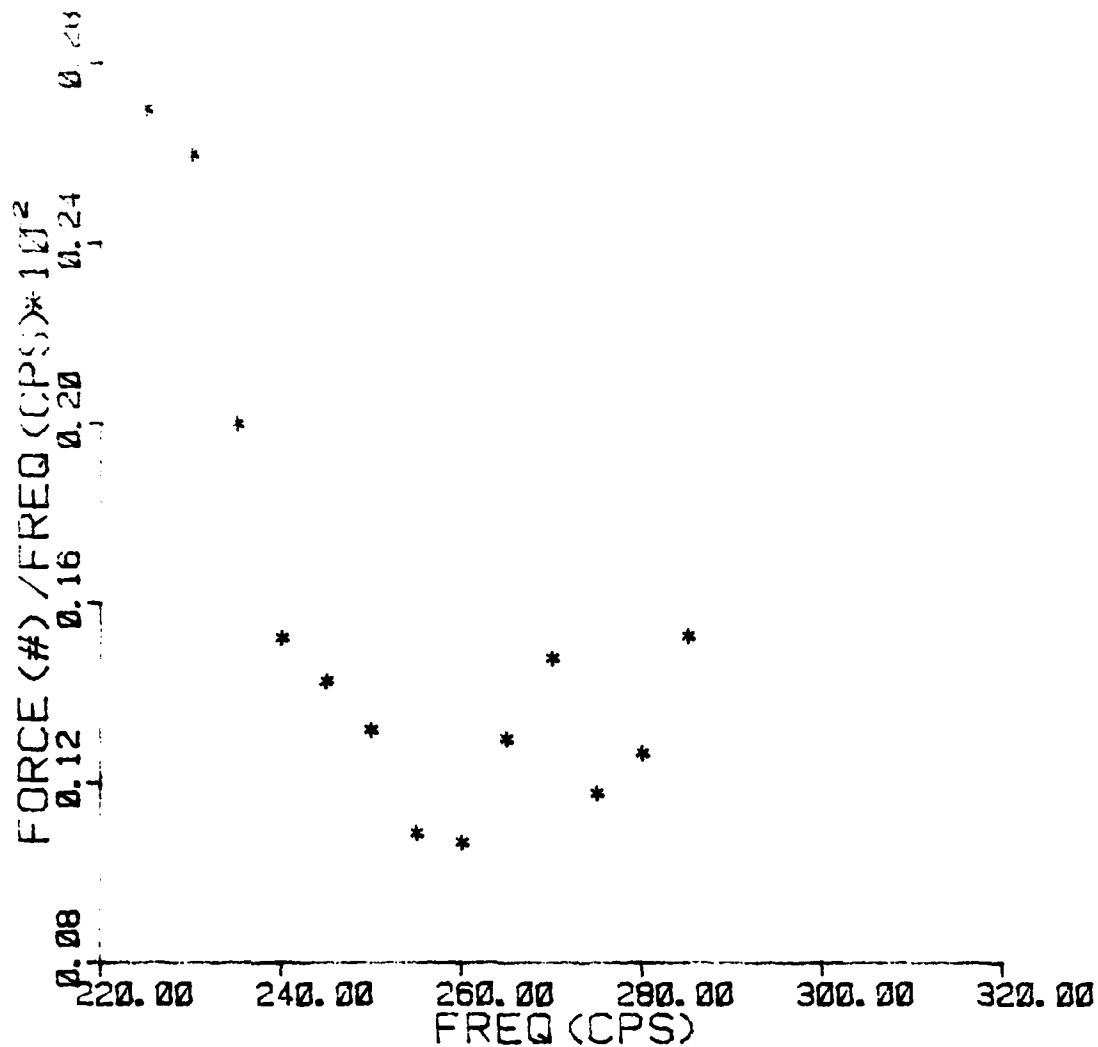
NARROWBAND FREQUENCY SWEEP FOR  
 DISPLACEMENT = 50  $\mu$  INCHES  
 (FREQUENCY VERSUS FORCE/FREQUENCY RUN 1)

FIGURE 12



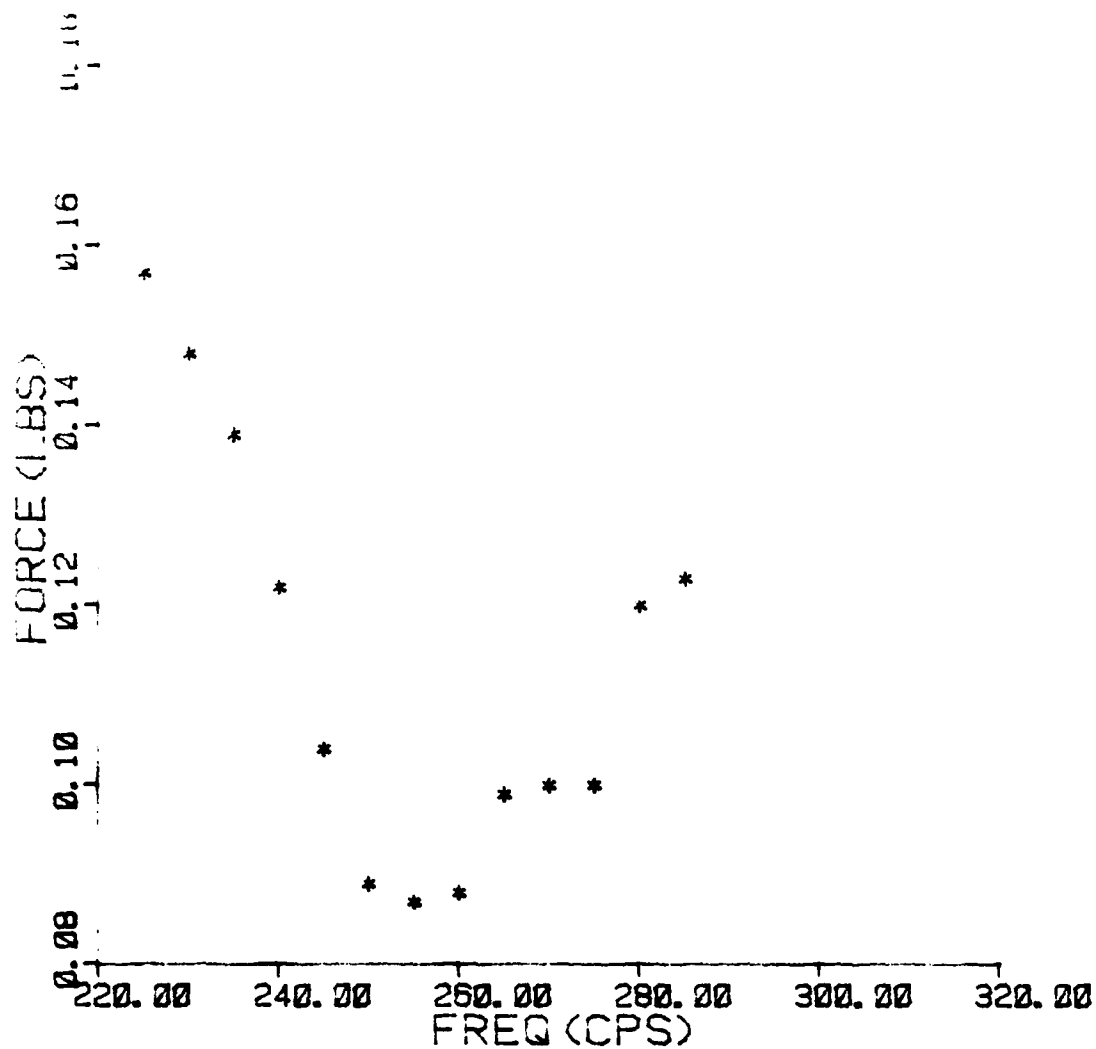
NARROWBAND FREQUENCY SWEEP FOR  
 DISPLACEMENT = 150  $\mu$  INCHES  
 (FREQUENCY VERSUS FORCE RUN1)

FIGURE 13



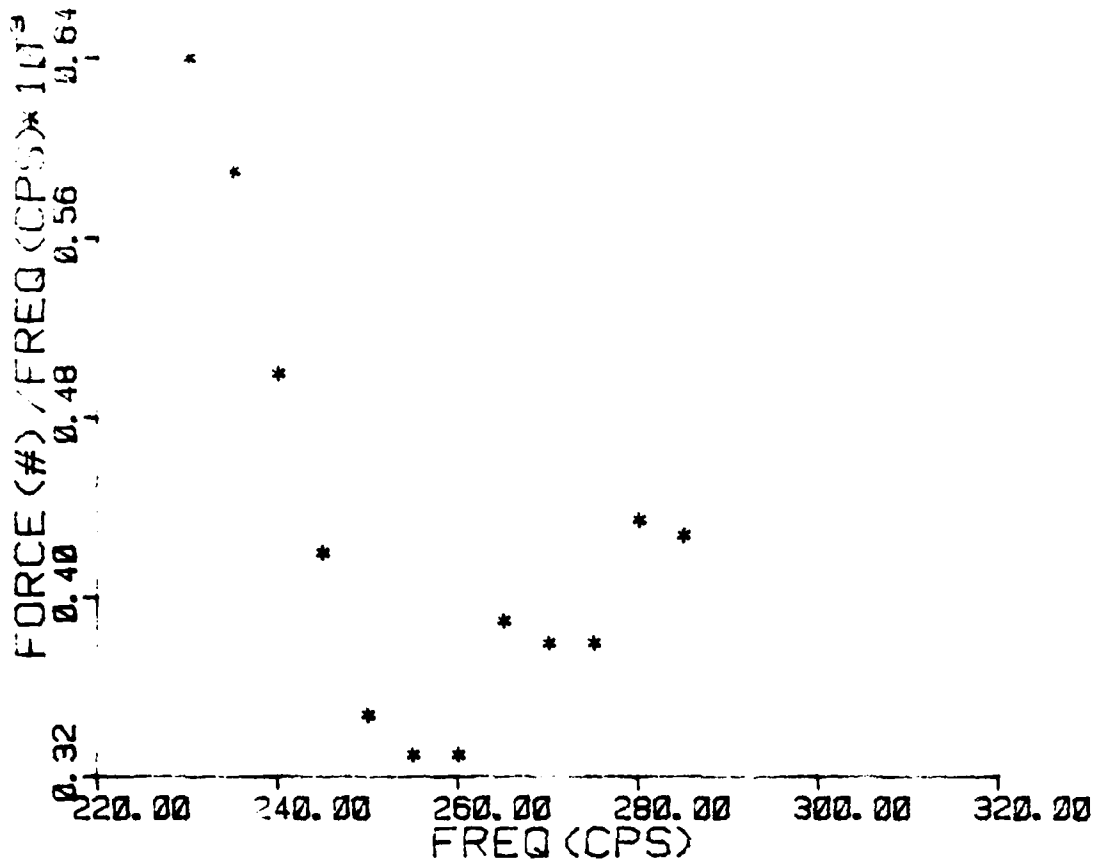
NARROWBAND FREQUENCY SWEEP FOR  
 DISPLACEMENT = 150  $\mu$  INCHES  
 (FREQUENCY VERSUS FORCE/FREQUENCY RUN1)

FIGURE 14



NARROWBAND FREQUENCY SWEEP FOR  
 DISPLACEMENT = 50  $\mu$  INCHES  
 (FREQUENCY VERSUS FORCE RUN2)

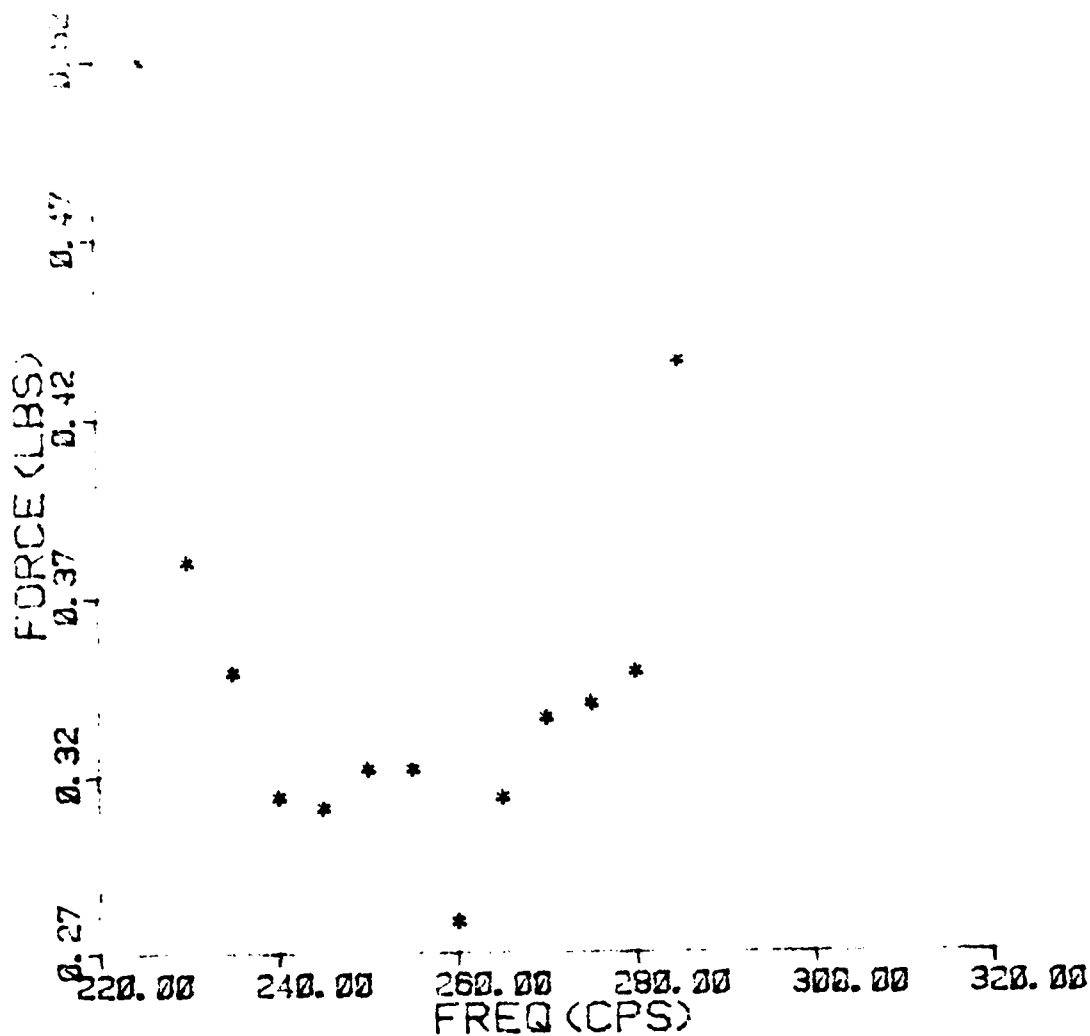
FIGURE 15



NARROWBAND FREQUENCY SWEEP FOR  
 DISPLACEMENT = 50  $\mu$  INCHES  
 (FREQUENCY VERSUS FORCE/FREQUENCY RUN 2)

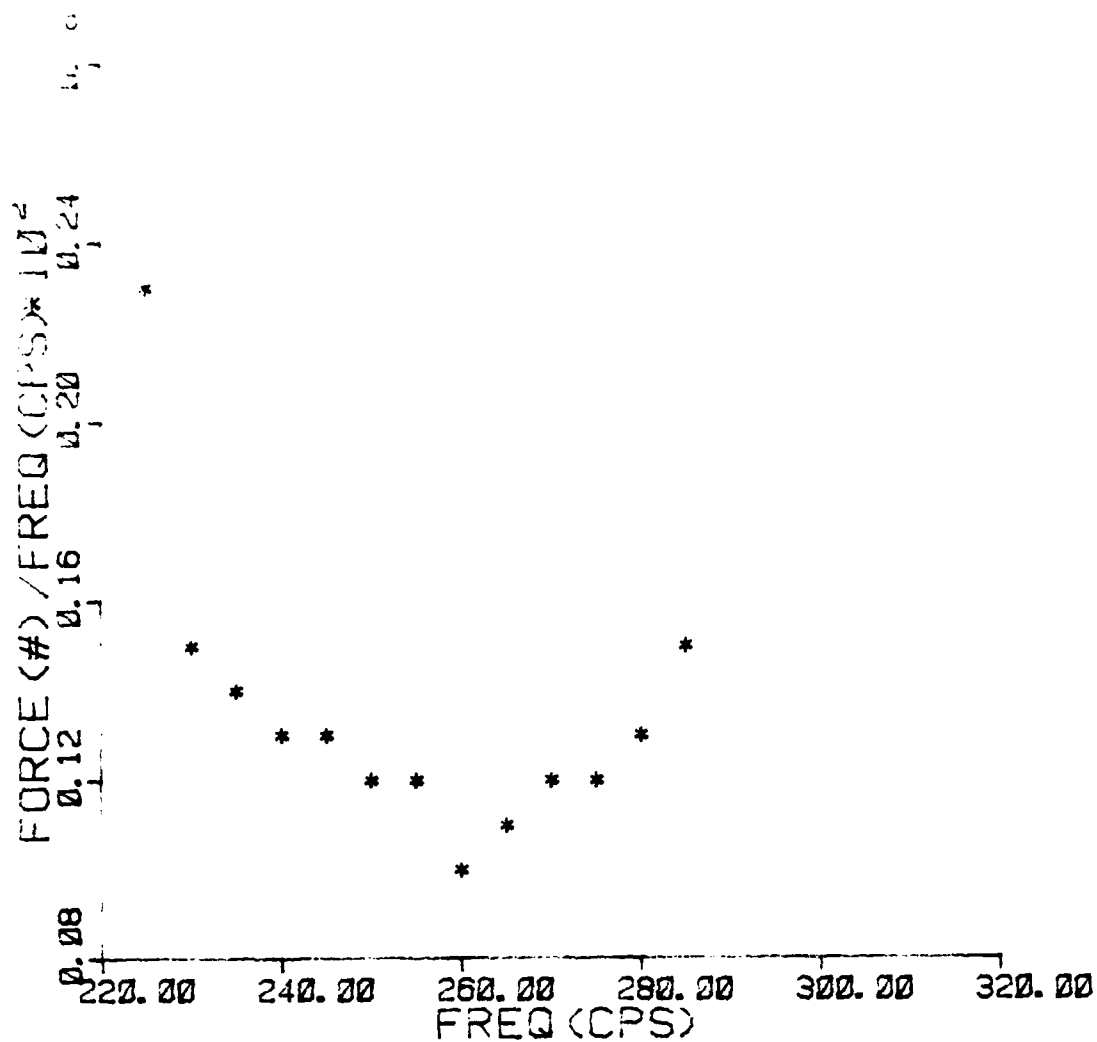
FIGURE 16





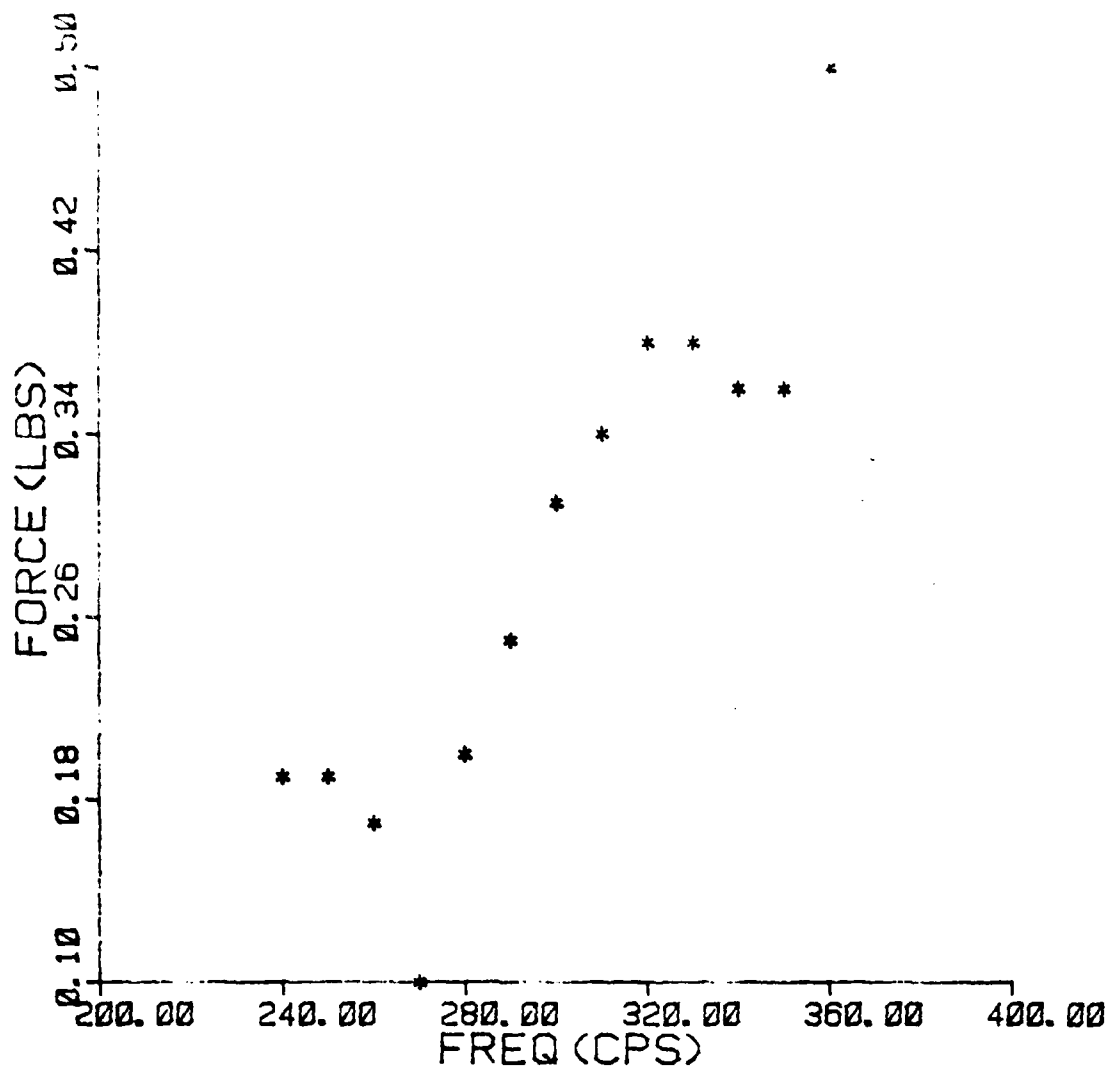
NARROWBAND FREQUENCY SWEEP FOR  
 DISPLACEMENT = 150  $\mu$  INCHES  
 (FREQUENCY VERSUS FORCE RUN2)

FIGURE 17



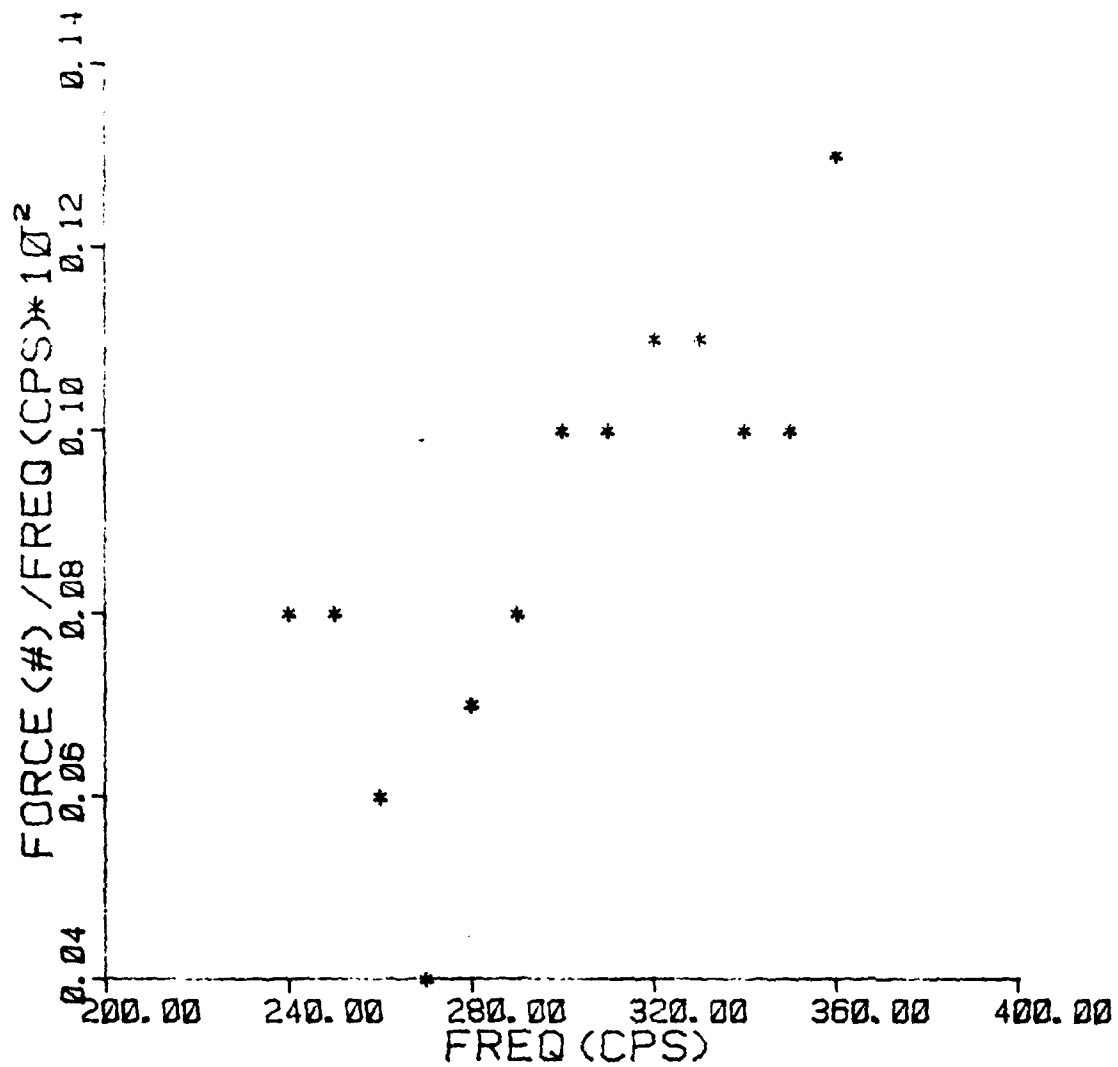
NARROWBAND FREQUENCY SWEEP FOR  
 DISPLACEMENT = 150  $\mu$  INCHES  
 (FREQUENCY VERSUS FORCE/FREQUENCY RUN2)

FIGURE 18



Narrowband Frequency Sweep  
Using Friction Damping  
For Displacement = 100  $\mu$  Inches  
(FREQUENCY VERSUS FORCE)

FIGURE 19



Narrowband Frequency Sweep  
 Using Friction Damping  
 For Displacement = 100  $\mu$  Inches  
 (FREQUENCY VERSUS FORCE/FREQUENCY)

FIGURE 20

### III Analytical Development

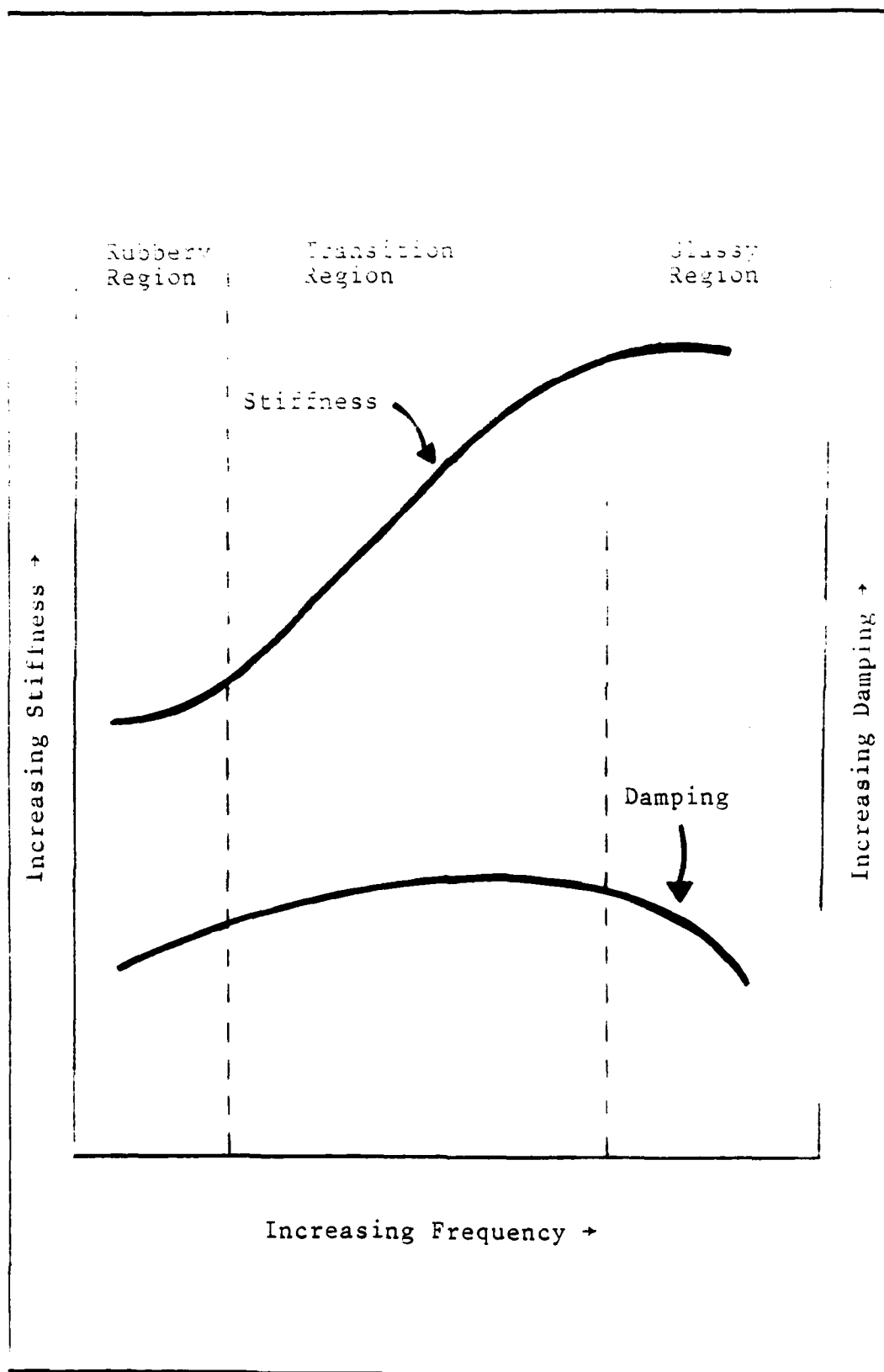
#### Model Description

The ultimate goal of the analytical section was to develop the equation of motion of the blade modeled in Figure 1. With this equation, the resulting eigenvalue problem can be solved and the resonant frequencies predicted, and hence, these predictions can be used as a check on experimentally determined data. However, because of the important properties of elastomers; the boundary condition at the root will be delineated in the next two sections, prior to the complete development of the beam equation.

#### Viscoelastic Properties

Figure 21 shows that both the stiffness and damping properties of elastomers vary with the frequency of a sinusoidal motion (Ref 2). A similar chart could be constructed to show that these properties also depend upon the temperature of the material. There are three discernible regions where the characteristic properties of the material can be described. However, since peak damping occurs in the transition region, it is this portion of the curve where the material is most effectively used as an energy dissipating device. The material used in this experiment, 101-111, has its peak damping at ambient temperature and in the frequency range of  $10^2$  to  $10^3$  cycles per second.

There are two primary methods of a bilinear model.



STIFFNESS AND DAMPING VERSUS FREQUENCY

FIGURE 21

material (Ref 2). The first is the fractional derivative technique. With this method, a derivative of order between zero and one is used in the differential equation of motion. The magnitude of the derivative is determined by the frequency dependence of the damping properties. The strongly dependent materials have a derivative near the first order and the weakly dependent elastomers would approach the zero order derivative. One advantage of this approach is that it can be used to model nonsinusoidal and transient excitations. However, it is mathematically more difficult than the other approach using the complex modulus.

Mathematical simplicity was the impetus for choosing the complex modulus to model the elastomer properties in this analysis. With this approach, the modulus used in the stress-strain relationship has two components: one real and one imaginary. It is written as follows:

$$\sigma = (E_1 + iE_2) \epsilon \quad (1)$$

$iE_2$  is the imaginary part or loss modulus and contains the dependence of the damping on the velocity, or the frequency of the vibrations. The following is an alternative form where  $\eta$  is the ratio of  $E_1$  and  $E_2$  called the loss factor:

$$\sigma = E_1(1 + i\eta) \epsilon \quad (2)$$

This model can only be used with pure sine wave excitations.

#### Boundary Conditions at the Root

To determine the boundary condition at the root of the

blade, (see Fig -), the moment at that point must be examined. Since the damping material will be stressed with a shearing force, the above tensile modulus must be changed to the shearing modulus. Then, as a result,

$$\tau = \frac{G \delta R}{t} = \frac{G R}{t} \frac{\partial y}{\partial x} \quad (3)$$

where

$$\frac{\partial y}{\partial x} = \text{slope of the beam at the root junction, and} \quad (4)$$

$$G = G_1(1 + in) \quad (5)$$

= complex shear modulus (lb/in<sup>2</sup>)

consequently the moment is

$$M = \tau(R \propto W)R = R^2 \propto W \tau \quad (6)$$

$$= \frac{c}{t} G_1(1 + in) \frac{\partial y}{\partial x} \quad (\text{See Fig 4}) \quad (7)$$

where

R = radius of blade root (inches)

$$c = 2R^3 \propto W \text{ (inches}^4\text{)} \quad (8)$$

W = width of blade (inches)

### Beam Equation

The classical cantilever beam equation is as follows

(Ref 3):

$$EI \frac{\partial^4 y}{\partial x^4} + M_b \frac{\partial^2 y}{\partial t^2} = 0 \quad (9)$$



where

$I = \text{moment of inertia of the blade in } \text{in}^4$

$E = \text{modulus of elasticity of the blade in } \text{psi}$

$y = \text{displacement of the blade in the transverse direction in in}$

$M_b = \text{mass per unit length of the blade } \text{lb sec}^2/\text{in}^2$

The following is the well-known solution to this equation

(Ref 4):

$$y(x,t) = (B_1 \sin \beta x + B_2 \cos \beta x + B_3 \sinh \beta x + B_4 \cosh \beta x) \sin \beta^2 a t \quad (10)$$

where

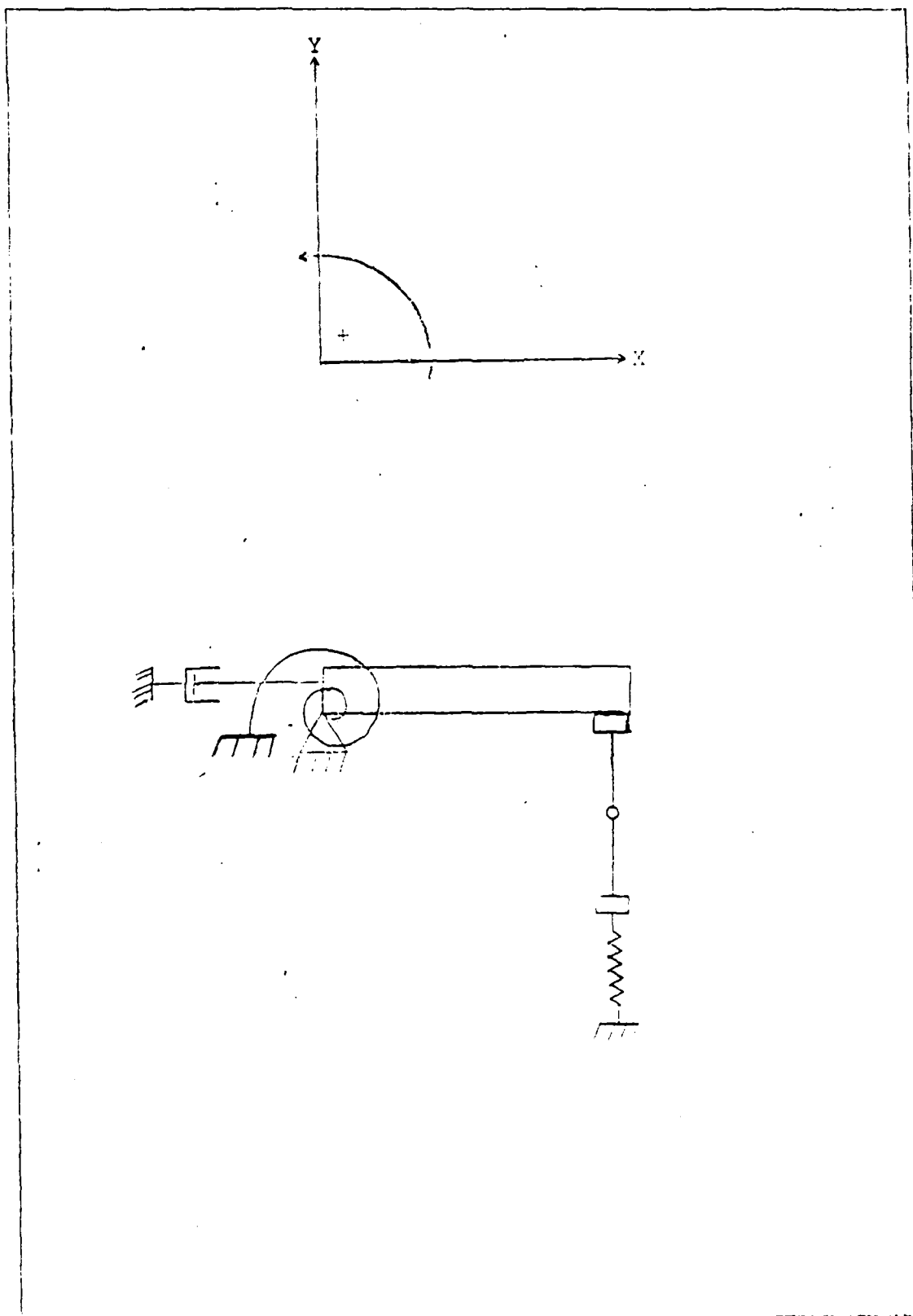
$$a = \sqrt{\frac{EI}{M_b}}$$

$\omega = \text{frequency of the response in radians per second, and}$

$$\beta^2 = \omega/a \quad (11)$$

### Boundary Conditions

Figure 22 delineates the boundary conditions of a modified cantilever beam. The bottom mass and stiffness at the tip represent the shaker and part of the linkage and force gauge. This is the source of the sinusoidal displacement. The top mass represents the remainder of the force gauge, linkage and accelerometer. The torsional spring and viscous damper at the root model the moment produced by the shearing force of the elastomer.



MODIFIED CANTILEVER BEAM AND SIGN CONVENTION

FIGURE 22

Consequently, the boundary conditions are:

$$(1) \quad y(0,t) = 0$$

$$(2) \quad EI \frac{\partial^2 y}{\partial x^2}(0,t) = \frac{c}{t} G_1 (1 + in) \frac{\partial y}{\partial x}(0,t)$$

$$(3) \quad EI \frac{\partial^2 y}{\partial x^2}(L,t) = 0$$

$$(4) \quad EI \frac{\partial^3 y}{\partial x^3}(L,t) - M_s \ddot{y}(L,t) - k_s y(L,t) = 0$$

From boundary condition (1)

$$B_4 = -B_2$$

From boundary condition (2)

$$EI(-B_2 \beta^2 + B_4 \beta^2) = \left[ \frac{c}{t} G_1 (1 + in) \right] [B_1 \beta + B_3 \beta]$$

$$\text{let } P = \frac{c}{t} G_1 (1 + in)$$

and substituting  $B_4 = -B_2$ , then

$$EI(2\beta B_4) = P(B_1 + B_3), \text{ or}$$

$$B_4 = \frac{P}{2EI\beta} (B_1 + B_3)$$

From boundary condition (3),

$$EI(-B_1 \beta^2 \sin \beta L - B_2 \beta^2 \cos \beta L + B_3 \beta^2 \sinh \beta L +$$

$$B_4 \beta^2 \cosh \beta L) = 0$$

Using previous substitutions and rearranging

$$B_3 \left[ \frac{P}{2EI\beta} (\cos \beta L + \cosh \beta L) + \sinh \beta L \right] =$$

$$B_1 \left[ \sin \beta L - \frac{P}{2EI\beta} (\cos \beta L + \cosh \beta L) \right]$$

$$\text{let } Q = \frac{P}{2EI\beta} (\cos \beta L + \cosh \beta L) + \sinh \beta L$$

$$\text{let } R = \sin \beta L - \frac{P}{2EI\beta} (\cos \beta L + \cosh \beta L)$$

$$\text{then } B_3 = B_1(R/Q)$$

From boundary condition (4)

$$EI \frac{\partial^3 y}{\partial x^3} (L, t) - M_s \ddot{y}(L, t) - k_s y(L, t) = 0$$

$$\text{where } \ddot{y}_L = -y_L (\beta^2 a)^2, \text{ then}$$

$$EI(-B_1 \beta^3 \cos \beta L + B_2 \beta^3 \sin \beta L + B_3 \beta^3 \cosh \beta L + B_4 \beta^3 \sinh \beta L) + \left[ M_s (\beta^2 a)^2 - k_s \right] (B_1 \sin \beta L + B_2 \cos \beta L + B_3 \sinh \beta L + B_4 \cosh \beta L) = 0$$

Using previous substitutions yields

$$EI(-B_1 \beta^3 \cos \beta L - \frac{P}{2EI\beta} (B_1 + B_1(R/Q)) \beta^3 \sin \beta L + B_1(R/Q) \beta^3 \cosh \beta L + \frac{P}{2EI\beta} (B_1 + B_1(R/Q)) \beta^3 \sinh \beta L + \left[ M_s (\beta^2 a)^2 - k_s \right] (B_1 \sin \beta L - \frac{P}{2EI\beta} (B_1 + B_1(R/Q)) \cos \beta L + B_1(R/Q) \sinh \beta L + \frac{P}{2EI\beta} (B_1 + B_1(R/Q)) \cosh \beta L) = 0$$

Factoring out  $E_1$  and rearranging yields the following eigenvalue problem with  $s$  as the eigenvalue:

$$\begin{aligned} -\cosh sL - \frac{P}{2EI_3} (1 + R/2) \sinh sL - \frac{P}{2EI_3} (1 + R/2) \cosh sL - \\ \frac{P}{2EI_3} (1 + R/2) \sinh sL + \frac{P}{2EI_3} (M_s + 3Pa_s^2 - k_s) \\ \left[ \sinh sL - \frac{P}{2EI_3} (1 + R/2) \cosh sL + (R/2) \sinh sL + \right. \\ \left. \frac{P}{2EI_3} (1 + R/2) \cosh sL \right] = 0 \end{aligned}$$

This problem was solved using an iterative technique delineated in Appendix C. Essentially, the technique consists of estimating a range of values for the real part of the eigenvalue and then incrementing the real part throughout this range searching for values of the function that are decreasing. When the function is minimized (ideally it would be equal to zero) the resulting real part of the eigenvalue is used to repeat the above procedure searching for the real and imaginary parts of the roots to the equation. In this case, the search range is determined for the complex part of the root.

One difficulty with this approach is that the resulting minimum value over a given range may not be an actual root of the equation. To overcome this difficulty, an order of magnitude analysis of each minimum, along with a comparison of eigenvalues of a pure cantilever beam, can be used to eliminate false roots.

There are canned programs available that will iterate roots of an equation. However, since the roots were complex, i.e. two dimensional, these programs were not used.

### Results

The following were the results of the above program for the boundary conditions depicted in Figure 21:

$$s_1 = (.1297, .0062)/in; \text{Complex Freq. } (26.2, 2.6)\text{cps}; G_1 = 43\text{psi}; n = .5$$

$$s_2 = (.4066, .0154)/in; \text{Complex Freq. } (258.3, 19.6)\text{cps}; G_1 = 138\text{psi}; n = 1.12$$

$$s_3 = (.6994, .017)/in; \text{Complex Freq. } (764.9, 37.4)\text{cps}; G_1 = 214\text{psi}; n = 1.17$$

In this case, the mass and stiffness of the shaker were removed along with part of the linkage mass. The remaining mass was  $0.000143 \text{ lbs} - \text{sec}^2/\text{in}^2$ , attributed to the linkage past the force gauge, one half the force gauge mass and the accelerometer mass.

The reason for including this mass in the configuration is that at resonance, the force should be at zero. Consequently, the mass and stiffness of the shaker along with part of the linkage was removed from the circuit. With these eigenvalues, the resulting frequencies were calculated using equation 11 and  $a/L^2 = .1$ . The following is a list of the values of the other parameters that entered into the equation for the frequencies:

$$\frac{PL}{EI} = \frac{(.6868/.00414)(43 + i 21.5)(10.5)}{31(10)^6(.001373)} = (1.76 + i .38) \text{ for } s_1$$

$$\frac{PL}{EI} = \frac{(.6868/.00414)(138 + i 154)(10.5)}{31(10)^6(.001373)} = (5.65 + i 6.30) \text{ for } s_2$$

$$\frac{PL}{EI} = \frac{(.6868/.00414)(214 + i 250)}{31(10)^6(.001373)} = (8.76 + i 10.24) \text{ for } s_3$$

$$\frac{Ms a^2}{EIL} = \frac{Ms}{M_0 L} = \frac{0.000143}{(.0004404)(10.5)} = 0.0309$$

$$\frac{k_s L^3}{EI} = \frac{0 (10.5)^3}{31(10)^6 (0.001373)} = 0$$

A comparison of the analytical and experimental results is as follows:

<u>Resonant Frequency</u>	<u>Analytical Prediction</u>	<u>Experimental Measurement</u>	<u>% Difference</u>
Second Run 1	258	255	1.1
Second Run 2	258	260	negligible
Third Run 1	764	775	1.4
Third Run 2	764	850	11

#### Analysis of Rigid Body Mode

Evidence of the lowest mode, expected to be predominantly a rigid body mode, with the viscoelastic spring restoring the mass, was not seen during the experiment. Consequently, separate analyses were undertaken to predict the frequency and response of this mode in an attempt to discover if the mode should have been observed.

The equation of motion for the rigid body analysis is as follows:

$$I_0 \ddot{\theta} = -\frac{mgL}{2} (1 + \sin\theta) \quad (12)$$

$I_0$  is the mass moment of inertia about the blade dovetail root made up of the mass of the blade and the tip mass described in the previous section. This tip mass is treated as a point mass; hence, the mass moment of inertia about its own center of gravity is ignored. In short,  $I_0$  is calculated as follows:

$$\begin{aligned}
I_o &= \frac{1}{3} M_b L^3 + M_t (L)^2 \\
&= \frac{1}{3} (0.0046)(10.5)^3 + 0.000143(10.5)^2 \\
&= 0.1348 \text{ lb} - \text{sec}^2 - \text{in}
\end{aligned}$$

Here the moment of inertia of the dovetail has been ignored.

The moment at the blade root is similar to equation 6 but for the rigid body mode  $\frac{\partial y}{\partial x}$  is replaced with  $y$ . Hence, the real part of the natural frequency for equation (12) is calculated as follows:

$$\omega^2 = \frac{cG_1}{I_o}$$

where  $G_1 = 43 \text{ lb/in}^2$  in this frequency range. Therefore, the frequency is as follows:

$$\begin{aligned}
\omega &= \left[ \frac{(.6868)(43)}{(0.1348)(0.000143)} \right]^{\frac{1}{2}} \\
&= 196.5 \text{ rad/sec} \\
&= 31.26 \text{ cps}
\end{aligned}$$

Since this frequency is close to the one predicted in the beam equation analysis -26.2 cps - it does not explain why it could not be found experimentally as a resonance .

As a final attempt to explain this enigma, an analytical prediction of the response was examined. The hypothesis was that if the damping in the rigid body mode was sufficiently heavy, then the dip in force at resonance may not be discernible. The analysis showed that this resonance should de-



limitedly be assumed: (a) that the magnitude of the response  
at the frequency in question shall be as small as not to  
exceed the noise level of the experimental work. For  
details of this analysis see in Appendix I.

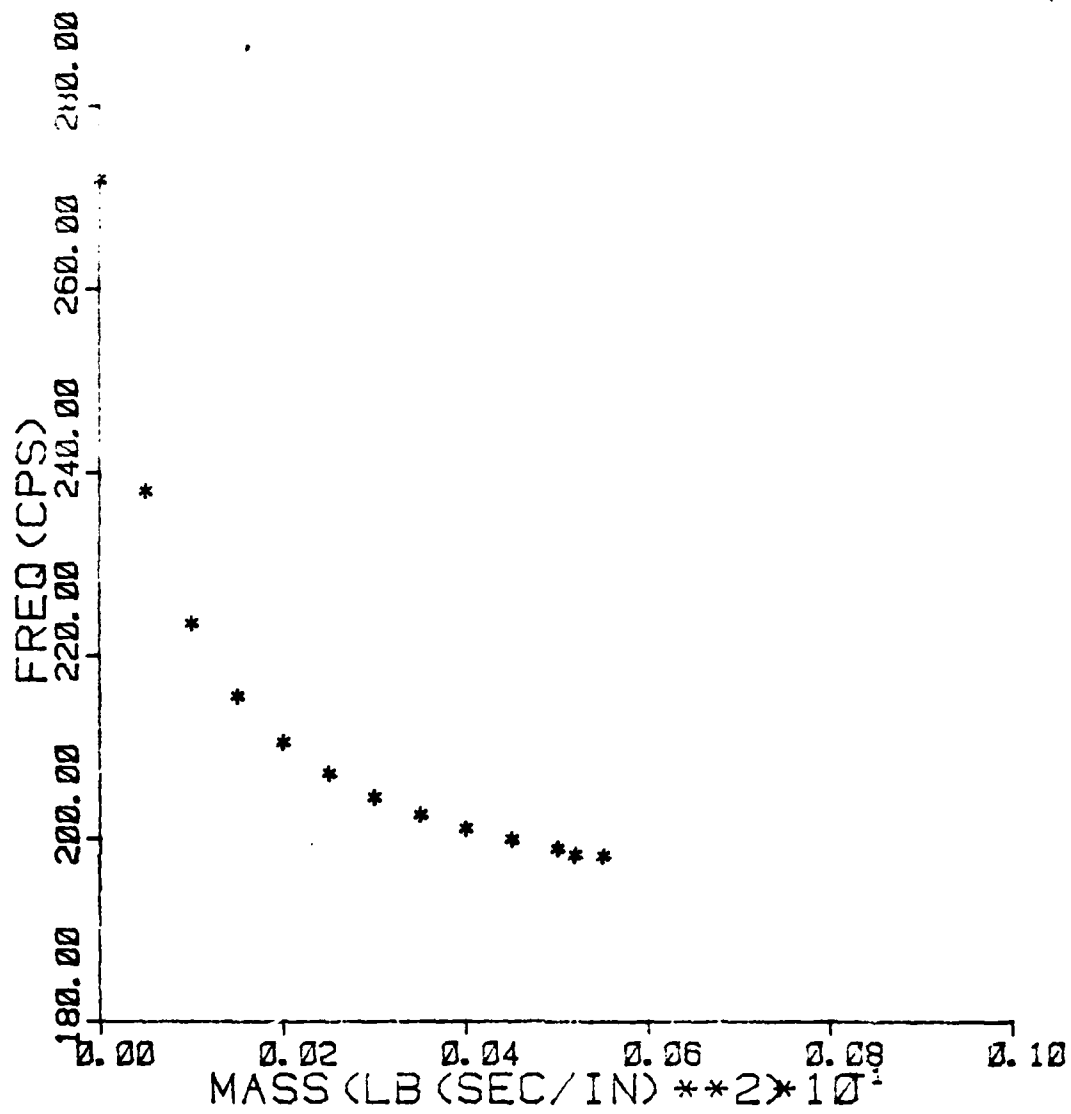
#### IV Sensitivity Analysis and Discussion

Several parameters in the experimental analysis were measured or determined with the inevitable possibility of human, and/or, equipment errors. In order to assess the impact of these possible errors, sensitivity analyses were performed on several of these parameters using the analytical model as a baseline. These parameters consisted of the thickness and complex modulus of the elastomer, the mass of the shaper, linkage, and rollers, and the various physical measurements of the blade model.

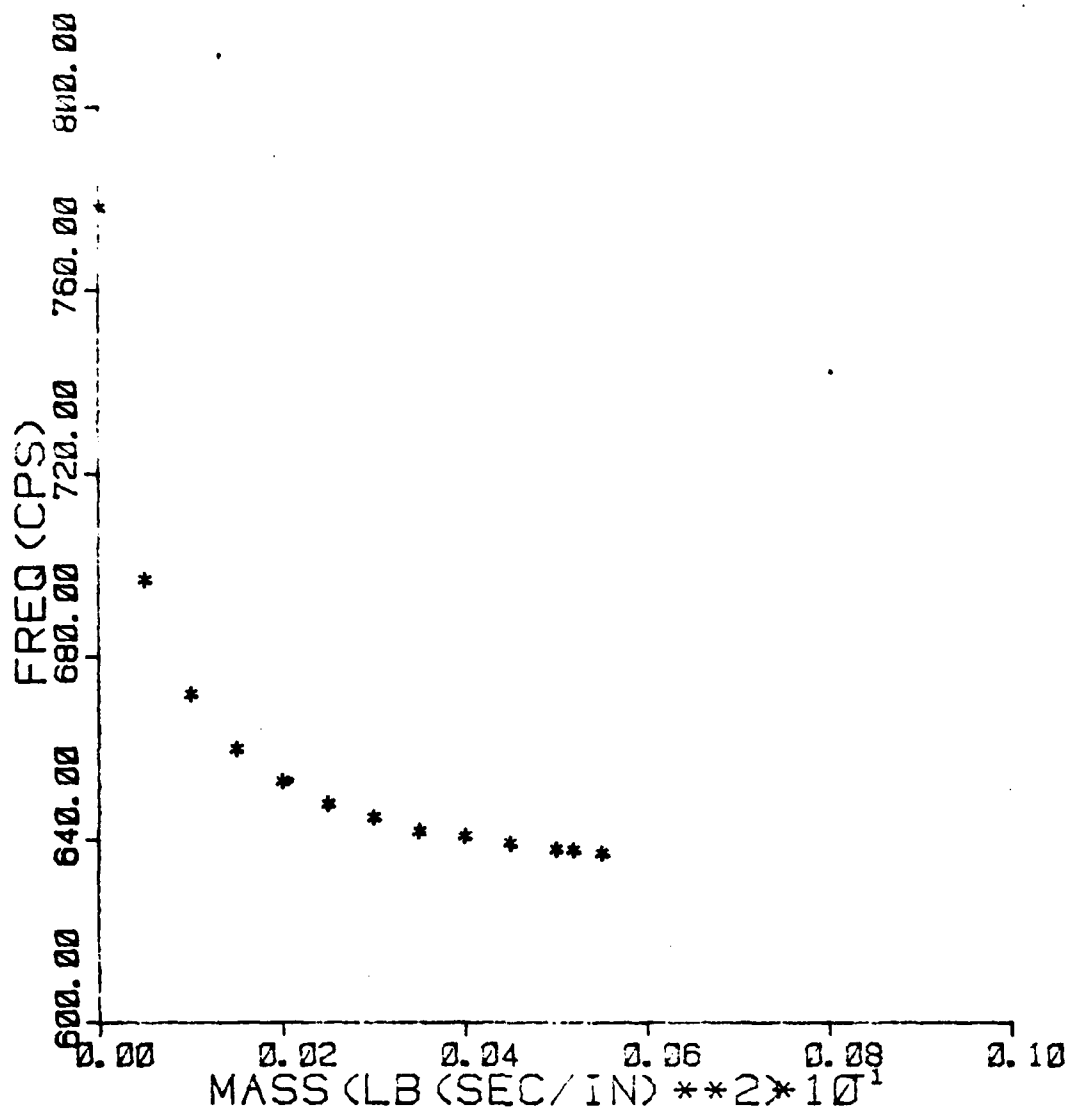
With two exceptions, most of the parameters were not sensitive enough to be a possible cause of large errors.

The first exception was the length of the blade. In this case, a 10% error in measurement would result in a 10% change in the analytically predicted resonant frequency. However, since the measurement can be made with a high degree of accuracy, it is not likely to cause problems.

The second exception was the tip mass. Figures 11 and 12 show that for tip masses less than 0.11 kg, the variation of predicted resonant frequencies are large. However, at resonance, the mass of the tip roller is eliminated, and as outlined in Appendix B, this is the most difficult portion of the tip mass to measure. The remaining most sensitive of the parameters is the mass of the shaper and linkage. It is shown in Figure 13 that a 10% error in the mass of the shaper and linkage results in a 10% change in the resonant frequency. It is not likely that this will be a problem.



TIP MASS VERSUS FREQUENCY  
 (Second Resonant Frequency)  
 FIGURE 23



TIP MASS VERSUS FREQUENCY

(Third Resonant Frequency)

FIGURE 24

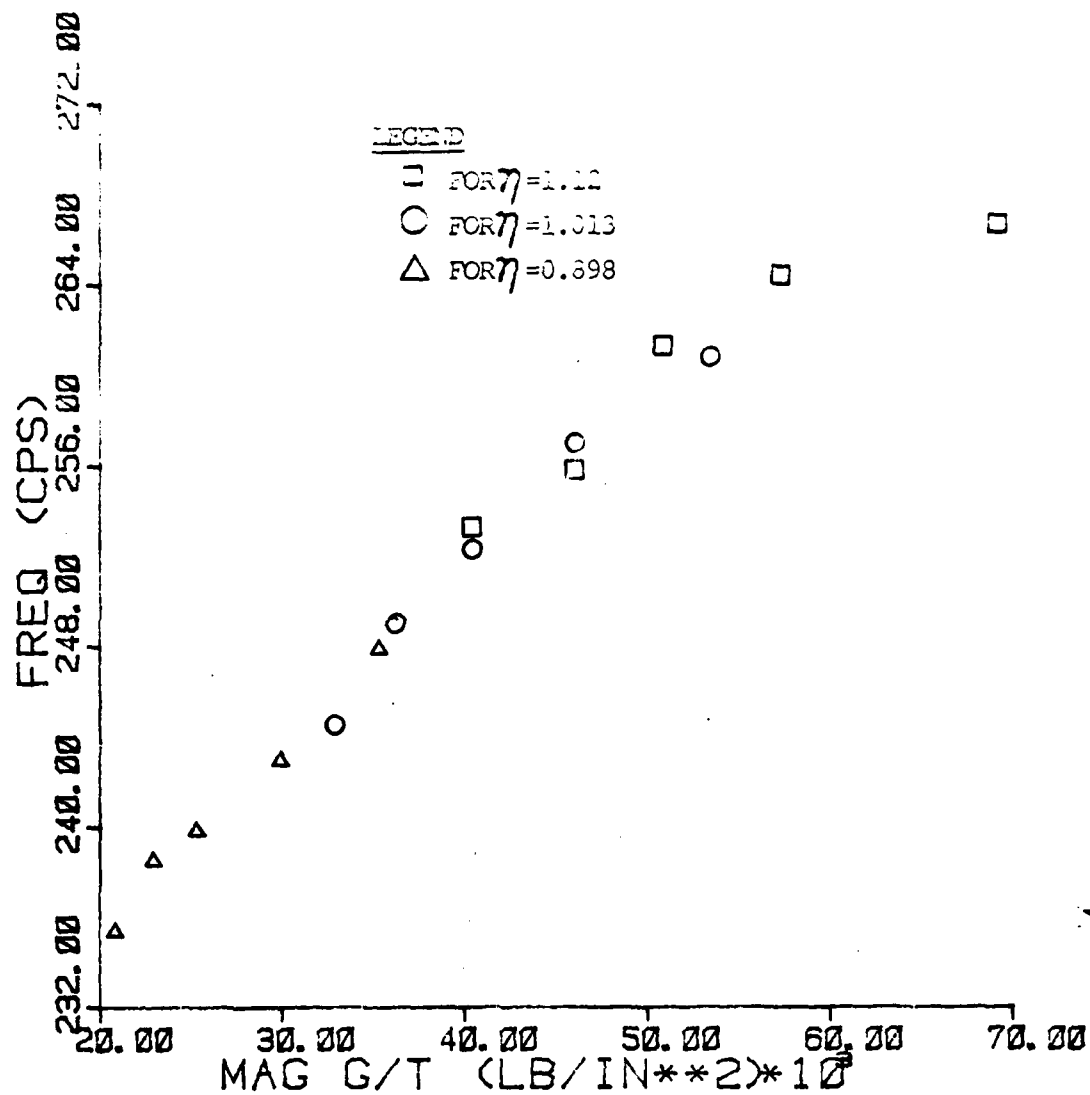
Two parameters that were difficult to measure were the elastomer thickness and temperature. The thickness presented difficulties because it was tedious trying to adjust the contact force to produce a symmetric thickness on both sides of the dovetail root. Also, during the approximate two hour period required to collect one data run, the thermocouple reading was observed to vary up to 10°F.

Figures 25 and 26 show the impact of the variances mentioned above. There are three different loss factors plotted to account for the temperature variations for both the second and third resonant frequencies. The data used for this comparison are as follows:

Loss Factor	Modulus (lbs/in <sup>2</sup> )	Temperature °C	Frequency (CPS)
$\eta_1 = 1.1203$	138	24.4	315.1
$\eta_2 = 1.0131$	117	29.4	304.4
$\eta_3 = .8981$	78	37.8	284.3

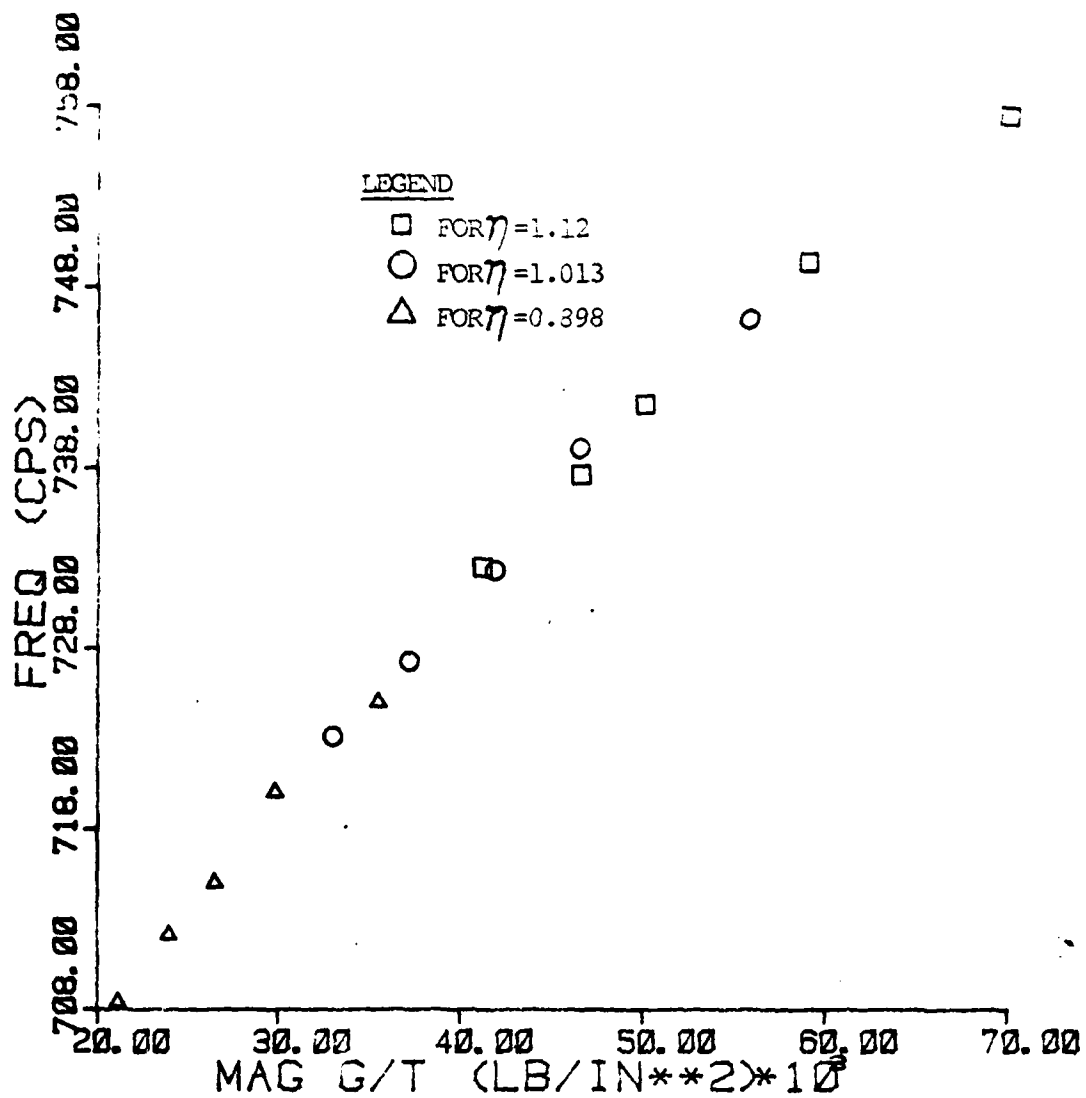
In addition, the elastomer thickness was varied from 0.003 to 0.005 inches. The abscissa is scaled to the magnitude of the complex modulus divided by the thickness.

Figure 25 shows that over the entire range of temperatures and thicknesses the predicted resulting frequency variation is less than 13%. Figure 26 shows that at the higher frequencies this error is reduced to less than 7%. In summary, variations in the above parameters will probably not cause large discrepancies in the results of the experiment.



MAGNITUDE OF MODULUS/THICKNESS  
 VERSUS FREQUENCY  
 (For Second Resonant Frequency)

FIGURE 25



MAGNITUDE OF MODULUS/THICKNESS  
 VERSUS FREQUENCY  
 (For Third Resonant Frequency)

FIGURE 26

## V Conclusion

In conclusion, viscoelastic materials appear promising as an effective vibration damper for turbine and compressor blades. Presently, most turbine engines use friction damping at the blade root of the turbine and compressor blades. By qualitatively comparing the flatness of response curves at resonance for friction and viscoelastic damping, the latter was found to have a flatter response. Hence, it appears to be a more effective damping mechanism. However, before this application can come to fruition, more research must be performed. Important questions must be answered. Questions such as: (1) "Is the increased complexity of a viscoelastic blade root material overcome by the benefits of improved vibration damping?" and (2) "Can a design be formulated which is serviceable in the adverse environment?"

Finally, this was intended to be a preliminary study. During the course of the study three other observations were made as follows:

(1) holding displacement constant while measuring the force is a feasible approach

(2) even though the analytical model is sensitive to tip mass, such a model can be made that correlates with experimental data at selected points

(3) if higher displacements had been used at the first resonant frequency the force measurements may have been greater than the noise level.



### Bibliography

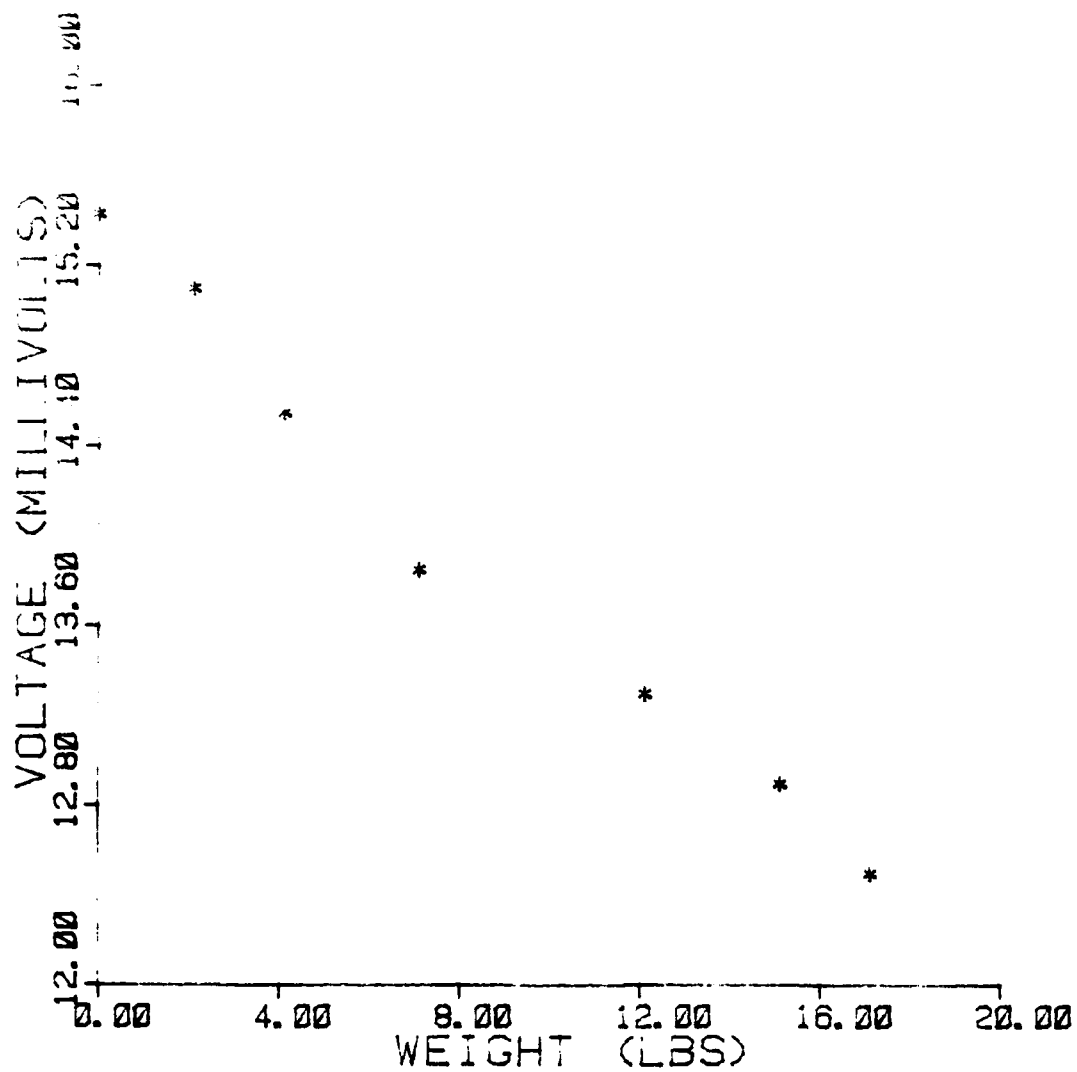
1. Ross, Daniel. Eric L. "Control of Plate Flexural Vibrations by Means of Viscoelastic Laminates." Structural Damping, ed. Jerome E. Adcock. ASME Colloquium, Atlantic City, NJ: December 1980.
2. Bagley, Ronald L. and Peter J. Torvik. "A Generalized Derivative Model for an Elastomer Damper." The Shock and Vibration Bulletin, No. 49, part 2, 135-143, September 1979.
3. Meirovitch, Leonard. Analytical Methods in Vibrations. London: Collier-Macmillan Limited. 162, 1967.
4. Meirovitch, Leonard. Elements of Vibration Analysis. New York: McGraw-Hill Book Company, 1975.
5. Bagley, Ronald L. "Fractional Calculus - A Different Approach to the Finite Element Analysis of Viscoelastically Damped Structures." AIAA/ASCE/AHS 22nd Structures, Structural Dynamics and Materials Conference, Atlanta, GA: 6 April 1981.
6. Balfour, A. and D.H. Marwick. Programming in Standard FORTRAN 77. New York: North-Holland Inc., 1979.
7. Bodynas, Richard G. Advanced Strength and Applied Stress Analysis. New York: McGraw-Hill Book Company, 1977.
8. Drake, Michael L. and Gary E. Terborg. Polymeric Material Testing Procedures to Determine Damping Properties and the Results of Selected Commercial Material. AFWAL-TR-80-4093, 1980.
9. Drake, Michael L., Robert J. Dominic and Binod Kumar. Evaluation of High Temperature Damping Applications to Increase Fatigue Life in Rotating Jet Engine Components. AFWAL-TR-80-4174, 1980.
10. Graves, George A., Charles Cannon, and Binod Kumar. A Study to Determine the Effect of Glass Compositional Variations on Vibration Damping Properties. AFWAL-TR-80-4061, 1980.
11. Hopkins, David M. and Michael L. Drake. Porcelain Enamel Material Testing Procedures to Determine the Damping Properties and the Results of Selected Materials. AFWAL-TR-80-4116, 1980.

12. Hill, Philip G. and Carl R. Peterson. Mechanics and Thermodynamics of Propulsion. Reading, Mass.: Addison-Wesley Publishing Company, 1970.
13. Mansergh, Michael G. Slip Damping of Turbine Vanes. AFIT Thesis, 1976.
14. Jones, David I. G. Vibrations of a Compressor Blade with Slip at the Root. AFWAL-TR-80-4003, 1980.
15. Jones, David I. G. Viscoelastic Materials for Damping Applications. AMD-701. 38 (1980): 17-51.

## Results

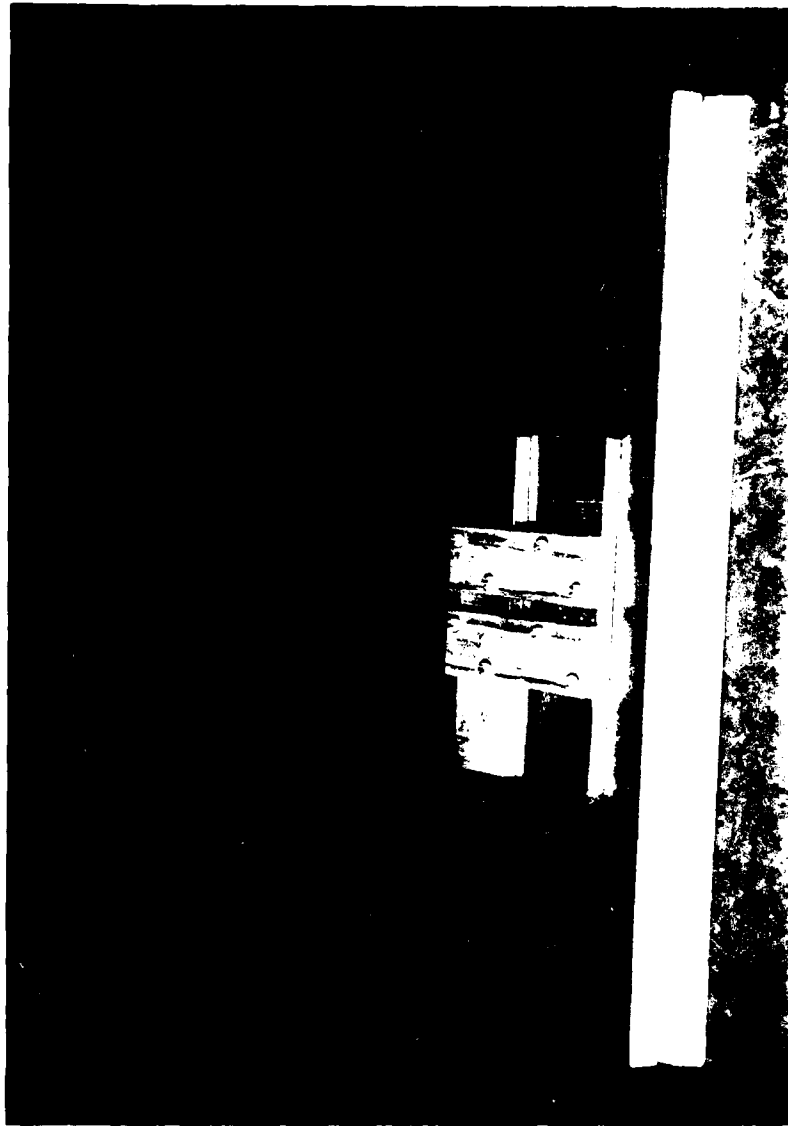
### Calibration of the Force Table

The spring beam (Fig. 5) was calibrated by placing a lead weight on the force table depicted in Figure 10 and Figure 13 and measuring the output voltage from the Wheatstone bridge. For each increase in weight, the force table guide was vibrated slightly by hand to eliminate any errors from friction and the corresponding voltages were recorded. Figure 27 is a plot of the resulting calibration curve. The resistor tolerances were not balanced out in the Wheatstone bridge; hence, as seen on the curve there is a voltage output with no applied force to the beam.



STRAIN GAUGE CALIBRATION CURVE

FIGURE 27



PICTURE OF TOWEL HOOK HUNG TO CHAIRBACK

FIGURE 23



PICTURE OF ENEMY TOWER IN POCKET

PICTURE 19

### Appendix B

#### Determination of Stiffness of the Shaker

The stiffness of the shaker was determined using the following formula:

$$k = F/D$$

where

k is the stiffness

F is a known force

D is a displacement

The procedure consisted of positioning the shaker so that the core motion was vertical. A known dead weight was balanced on the tip of the element and the displacement was measured with the Gaertner microscope, so that a stiffness could be computed.

Next, an accelerometer was mounted on the tip of the element. Using an appropriate amplifier, the accelerometer output was connected to a brush recorder model RD 2522 20. The shaker was given a brisk impulse and the output of the oscillations were recorded on the Brush recorder. With the recorded calibrated time axis, the fundamental frequency of oscillation was determined. Then using using the formula:

$$M = \frac{k}{\omega_n^2}$$

where

$\omega_n$  is the natural frequency

k is the stiffness determined above

$M_s'$  is the mass of the shaker, connecting  
bolt and accelerometer

the moving mass of the shaker with the accelerometer and connecting bolt was calculated from the formula and the measured stiffness. The accelerometer was weighed and its mass was subtracted from the calculated total. Since the connecting bolt remained on the shaker for all the experimental tests, its mass was not subtracted from the total. The resulting values are as follows:

$$k = 11.54 \text{ lb/in}^2$$

$$\omega_n = 11.5 \text{ cps} = 72.26 \text{ rad/sec}$$

$$M_s = M_s' - \text{accelerometer mass} \\ = 0.002048 \text{ lb-sec}^2/\text{in}$$



## Appendix 2

### Iterative Solution to Eigenvalue Problem

The following Fortran II program was used to determine the eigenvalues for the equation of motion. The thickness and complex shear modulus are input interactively in order to facilitate sensitivity analyses. The iteration increments and eigenvalue ranges are input interactively to insure that the program converges to each eigenvalue without passing over any.

In the first half of the program, the imaginary parts of the complex arguments are set to zero to obtain a rough estimate of the real part of the eigenvalue. With this estimate, the second part of the program iterates on both the real and imaginary parts of the actual eigenvalue. Then, the range of the eigenvalue estimate is increased and the above procedure is repeated for the next eigenvalue.

```
PROGRAM EQROOT
C THIS PROGRAM IS DESIGNED TO ITERATE TO SOLUTIONS OF THE
C EIGENVALUE PROBLEM RESULTING FROM THE EQUATION OF
C MOTION IN THE ANALYTICAL SECTION
REAL G1,G2,C,T,L,M,K,J,F1,F2,F3,F4,X1,X2
COMPLEX Z,Z1,B,D,F,W
COMMON G1,G2,C,T,L,M,K,J,A,Z1,W
Z1=(0.0,1.0)
C=(2.5)*(0.496**3.0)*(2.2514)
C C IS THE CONSTANT FROM EQUATION 7
L=10.5
C L IS THE LENGTH OF THE BLADE
M=0.002458
C M IS THE MASS OF THE SHAKER, LINKAGE, FORCE GAUGE AND
C ACCELEROMETER
K=11.54
C K IS THE STIFFNESS OF THE SHAKER
J=31*(10.0**6)*(0.001373)
```



```

F1=REAL(F/B)
F2=AIMAG(F/B)
F3=1.0+1.0*AIMAG(D)
F4=1.0+1.0*REAL(D)
F5=1.0+1.0*REAL(D)**2.0+1.0*AIMAG(D)**2.0
F6=1.0+1.0*REAL(D)**2.0+1.0*AIMAG(D)**2.0
F7=1.0+1.0*REAL(D)**2.0+1.0*AIMAG(D)**2.0
F8=1.0+1.0*REAL(D)**2.0+1.0*AIMAG(D)**2.0
F9=1.0+1.0*REAL(D)**2.0+1.0*AIMAG(D)**2.0
F10=1.0+1.0*REAL(D)**2.0+1.0*AIMAG(D)**2.0
F11=1.0+1.0*REAL(D)**2.0+1.0*AIMAG(D)**2.0
F12=1.0+1.0*REAL(D)**2.0+1.0*AIMAG(D)**2.0
F13=1.0+1.0*REAL(D)**2.0+1.0*AIMAG(D)**2.0
F14=1.0+1.0*REAL(D)**2.0+1.0*AIMAG(D)**2.0
F15=1.0+1.0*REAL(D)**2.0+1.0*AIMAG(D)**2.0
F16=1.0+1.0*REAL(D)**2.0+1.0*AIMAG(D)**2.0
F17=1.0+1.0*REAL(D)**2.0+1.0*AIMAG(D)**2.0
F18=1.0+1.0*REAL(D)**2.0+1.0*AIMAG(D)**2.0
F19=1.0+1.0*REAL(D)**2.0+1.0*AIMAG(D)**2.0
F20=1.0+1.0*REAL(D)**2.0+1.0*AIMAG(D)**2.0
F21=1.0+1.0*REAL(D)**2.0+1.0*AIMAG(D)**2.0
F22=1.0+1.0*REAL(D)**2.0+1.0*AIMAG(D)**2.0
F23=1.0+1.0*REAL(D)**2.0+1.0*AIMAG(D)**2.0
F24=1.0+1.0*REAL(D)**2.0+1.0*AIMAG(D)**2.0
F25=1.0+1.0*REAL(D)**2.0+1.0*AIMAG(D)**2.0
F26=1.0+1.0*REAL(D)**2.0+1.0*AIMAG(D)**2.0
F27=1.0+1.0*REAL(D)**2.0+1.0*AIMAG(D)**2.0
F28=1.0+1.0*REAL(D)**2.0+1.0*AIMAG(D)**2.0
F29=1.0+1.0*REAL(D)**2.0+1.0*AIMAG(D)**2.0
F30=1.0+1.0*REAL(D)**2.0+1.0*AIMAG(D)**2.0
F31=1.0+1.0*REAL(D)**2.0+1.0*AIMAG(D)**2.0
F32=1.0+1.0*REAL(D)**2.0+1.0*AIMAG(D)**2.0
F33=1.0+1.0*REAL(D)**2.0+1.0*AIMAG(D)**2.0
F34=1.0+1.0*REAL(D)**2.0+1.0*AIMAG(D)**2.0
F35=1.0+1.0*REAL(D)**2.0+1.0*AIMAG(D)**2.0
F36=1.0+1.0*REAL(D)**2.0+1.0*AIMAG(D)**2.0
F37=1.0+1.0*REAL(D)**2.0+1.0*AIMAG(D)**2.0
F38=1.0+1.0*REAL(D)**2.0+1.0*AIMAG(D)**2.0
F39=1.0+1.0*REAL(D)**2.0+1.0*AIMAG(D)**2.0
F40=1.0+1.0*REAL(D)**2.0+1.0*AIMAG(D)**2.0
F41=1.0+1.0*REAL(D)**2.0+1.0*AIMAG(D)**2.0
F42=1.0+1.0*REAL(D)**2.0+1.0*AIMAG(D)**2.0
F43=1.0+1.0*REAL(D)**2.0+1.0*AIMAG(D)**2.0
F44=1.0+1.0*REAL(D)**2.0+1.0*AIMAG(D)**2.0
F45=1.0+1.0*REAL(D)**2.0+1.0*AIMAG(D)**2.0
F46=1.0+1.0*REAL(D)**2.0+1.0*AIMAG(D)**2.0
F47=1.0+1.0*REAL(D)**2.0+1.0*AIMAG(D)**2.0
F48=1.0+1.0*REAL(D)**2.0+1.0*AIMAG(D)**2.0
F49=1.0+1.0*REAL(D)**2.0+1.0*AIMAG(D)**2.0
F50=1.0+1.0*REAL(D)**2.0+1.0*AIMAG(D)**2.0
F51=1.0+1.0*REAL(D)**2.0+1.0*AIMAG(D)**2.0
F52=1.0+1.0*REAL(D)**2.0+1.0*AIMAG(D)**2.0
F53=1.0+1.0*REAL(D)**2.0+1.0*AIMAG(D)**2.0
F54=1.0+1.0*REAL(D)**2.0+1.0*AIMAG(D)**2.0
F55=1.0+1.0*REAL(D)**2.0+1.0*AIMAG(D)**2.0
F56=1.0+1.0*REAL(D)**2.0+1.0*AIMAG(D)**2.0
F57=1.0+1.0*REAL(D)**2.0+1.0*AIMAG(D)**2.0
F58=1.0+1.0*REAL(D)**2.0+1.0*AIMAG(D)**2.0
F59=1.0+1.0*REAL(D)**2.0+1.0*AIMAG(D)**2.0
F60=1.0+1.0*REAL(D)**2.0+1.0*AIMAG(D)**2.0
F61=1.0+1.0*REAL(D)**2.0+1.0*AIMAG(D)**2.0
F62=1.0+1.0*REAL(D)**2.0+1.0*AIMAG(D)**2.0
F63=1.0+1.0*REAL(D)**2.0+1.0*AIMAG(D)**2.0
F64=1.0+1.0*REAL(D)**2.0+1.0*AIMAG(D)**2.0
F65=1.0+1.0*REAL(D)**2.0+1.0*AIMAG(D)**2.0
F66=1.0+1.0*REAL(D)**2.0+1.0*AIMAG(D)**2.0
F67=1.0+1.0*REAL(D)**2.0+1.0*AIMAG(D)**2.0
F68=1.0+1.0*REAL(D)**2.0+1.0*AIMAG(D)**2.0
F69=1.0+1.0*REAL(D)**2.0+1.0*AIMAG(D)**2.0
F70=1.0+1.0*REAL(D)**2.0+1.0*AIMAG(D)**2.0
F71=1.0+1.0*REAL(D)**2.0+1.0*AIMAG(D)**2.0
F72=1.0+1.0*REAL(D)**2.0+1.0*AIMAG(D)**2.0
F73=1.0+1.0*REAL(D)**2.0+1.0*AIMAG(D)**2.0
F74=1.0+1.0*REAL(D)**2.0+1.0*AIMAG(D)**2.0
F75=1.0+1.0*REAL(D)**2.0+1.0*AIMAG(D)**2.0
F76=1.0+1.0*REAL(D)**2.0+1.0*AIMAG(D)**2.0
F77=1.0+1.0*REAL(D)**2.0+1.0*AIMAG(D)**2.0
F78=1.0+1.0*REAL(D)**2.0+1.0*AIMAG(D)**2.0
F79=1.0+1.0*REAL(D)**2.0+1.0*AIMAG(D)**2.0
F80=1.0+1.0*REAL(D)**2.0+1.0*AIMAG(D)**2.0
F81=1.0+1.0*REAL(D)**2.0+1.0*AIMAG(D)**2.0
F82=1.0+1.0*REAL(D)**2.0+1.0*AIMAG(D)**2.0
F83=1.0+1.0*REAL(D)**2.0+1.0*AIMAG(D)**2.0
F84=1.0+1.0*REAL(D)**2.0+1.0*AIMAG(D)**2.0
F85=1.0+1.0*REAL(D)**2.0+1.0*AIMAG(D)**2.0
F86=1.0+1.0*REAL(D)**2.0+1.0*AIMAG(D)**2.0
F87=1.0+1.0*REAL(D)**2.0+1.0*AIMAG(D)**2.0
F88=1.0+1.0*REAL(D)**2.0+1.0*AIMAG(D)**2.0
F89=1.0+1.0*REAL(D)**2.0+1.0*AIMAG(D)**2.0
F90=1.0+1.0*REAL(D)**2.0+1.0*AIMAG(D)**2.0
F91=1.0+1.0*REAL(D)**2.0+1.0*AIMAG(D)**2.0
F92=1.0+1.0*REAL(D)**2.0+1.0*AIMAG(D)**2.0
F93=1.0+1.0*REAL(D)**2.0+1.0*AIMAG(D)**2.0
F94=1.0+1.0*REAL(D)**2.0+1.0*AIMAG(D)**2.0
F95=1.0+1.0*REAL(D)**2.0+1.0*AIMAG(D)**2.0
F96=1.0+1.0*REAL(D)**2.0+1.0*AIMAG(D)**2.0
F97=1.0+1.0*REAL(D)**2.0+1.0*AIMAG(D)**2.0
F98=1.0+1.0*REAL(D)**2.0+1.0*AIMAG(D)**2.0
F99=1.0+1.0*REAL(D)**2.0+1.0*AIMAG(D)**2.0
F100=1.0+1.0*REAL(D)**2.0+1.0*AIMAG(D)**2.0

```

40 IF(AIMAG(D).LT.0.0001)THEN  
 DO TO 50  
 END IF  
 F1=REAL(F/B)  
 F2=AIMAG(F/B)  
 B=B+REAL(D)  
 F3=REAL(F/B)  
 F4=AIMAG(F/B)  
 IF(F1\*\*2.0+F2\*\*2.0.GE.F3\*\*2.0+F4\*\*2.0) THEN  
 DO TO 40  
 END IF  
 B=B-2.0\*(REAL(D))  
 D=D/10  
 DO TO 30  
 50 PRINT\*, 'B=', B  
 W=(A\*B\*\*2.0)/(2.0\*3.1416)  
 PRINT\*, 'W=', W  
 PRINT\*, 'F1=', F1  
 PRINT\*, 'F2=', F2  
 PRINT\*, 'F3=', F3  
 PRINT\*, 'F4=', F4  
 END IF  
 END  
 COMPLEX FUNCTION F(Z)  
 C THIS FUNCTION COMPUTES A VALUE FOR THE EQUATION OF  
 C MOTION THAT SHOULD CONVERGE TO ZERO TO SOLVE THE  
 C EIGENVALUE PROBLEM  
 COMMON G1,G2,C,T,L,M,K,J,A,Z1,W  
 COMPLEX Z,Z1,B,W,Y  
 REAL G1,G2,C,T,L,M,K,J,A,D,X  
 COMPLEX P,R,Q  
 Z=Z\*L  
 P=(C/T)\*(G1+Z1\*G2)  
 R=CSIN(Z)-(CCOS(Z)+CCOSH(Z))\*(P/(2.0\*J\*(Z/L)))  
 Q=CSINH(Z)+(CCOS(Z)+CCOSH(Z))\*(P/(2.0\*J\*(Z/L)))  
 F=-CCOS(Z)-(P/(2.0\*J\*(Z/L)))\*(1.0+R/Q)\*CSIN(Z)  
 \*(R/Q)\*CCOSH(Z)+(P/(2.0\*J\*(Z/L)))\*(1.0+R/Q)\*CSINH(Z)  
 \*(1.0/(J\*(Z/L)\*\*3.0))\*(M\*(A\*(Z/L)\*\*2.0)\*\*2.0  
 \*-K)\*(CSIN(Z)-(P/(2.0\*J\*(Z/L)))\*(1.0+R/Q)\*CCOS(Z)+  
 \*(R/Q)\*CSINH(Z)+(P/(2.0\*J\*(Z/L)))\*(1.0+R/Q)\*CCOSH(Z))  
 Z=Z/L  
 END  
 COMPLEX FUNCTION CSINH(Z)  
 C THIS FUNCTION COMPUTES A VALUE FOR THE COMPLEX

```

1  HYPERBOLIC SINE
   COMPLEX Z
   PARAMETER I= 0,1
   X=REAL(Z)
   Y=AIMAG(Z)
   ZSINH= SINH(X)*COS(Y)+I*COSH(X)*SIN(Y)
   END
2  COMPLEX FUNCTION COSH Z
   THIS FUNCTION COMPUTES A VALUE FOR THE COMPLEX
   HYPERBOLIC COSINE
   COMPLEX Z
   PARAMETER I= 0,1
   X=REAL(Z)
   Y=AIMAG(Z)
   ZCOSH=COSH(X)*COS(Y)+I*SINH(X)*SIN(Y)
   END

```

## Appendix D

### Response Analysis of Rigid Body Mode

The equation of motion for a rigid body with viscous damping and harmonic excitation is as follows (Ref 4):

$$m\ddot{y}(t) + k(1 + i\gamma) y(t) = Ake^{i\omega t} \quad (13)$$

Assuming  $y(t) = Be^{i\omega t} = B \cos \omega t + Bi \sin \omega t$   
then

$$-\omega^2 Bme^{i\omega t} + k(1 + i\gamma) Be^{i\omega t} = Ake^{i\omega t}$$

or

$$B = \frac{Ak}{k(1 + i\gamma) - \omega^2 m} = \frac{A}{1 + i\gamma - \omega^2 (m/k)}$$

but  $\frac{m}{k} = \frac{1}{\omega_n^2}$ , therefore

$$B = \frac{A}{1 + i\gamma - \frac{\omega^2}{\omega_n^2}}$$

The amplitude of the steady state displacement is

$$|y| = B$$

then

$$|y| = \frac{|A|}{|1 + i\gamma - (\frac{\omega}{\omega_n})^2|} = \frac{|A|}{((1 - (\omega/\omega_n)^2)^2 + \gamma^2)^{1/2}} \quad (14)$$

In order to match the physics of the turbine blade problem, equation (13) should be

$$I_0 \ddot{\phi} + G_1 (c/t)(1 + i\gamma) \phi = M(t) = F_0 L e^{i\omega t}$$

but, the following parameters can be substituted:

$$y \rightarrow \phi L$$

$$k \rightarrow G_1 (c/t)$$

$$m \rightarrow I_0$$

$$Ak = F_0 L^2$$

$$\gamma = \eta$$

Consequently, equation (14) can be written as

$$F_0 = \frac{G_1 (c/t)}{L^2} \left[ (1 - \omega^2/\omega_n^2)^2 + \eta^2 \right]^{1/2} |y| \quad (15)$$

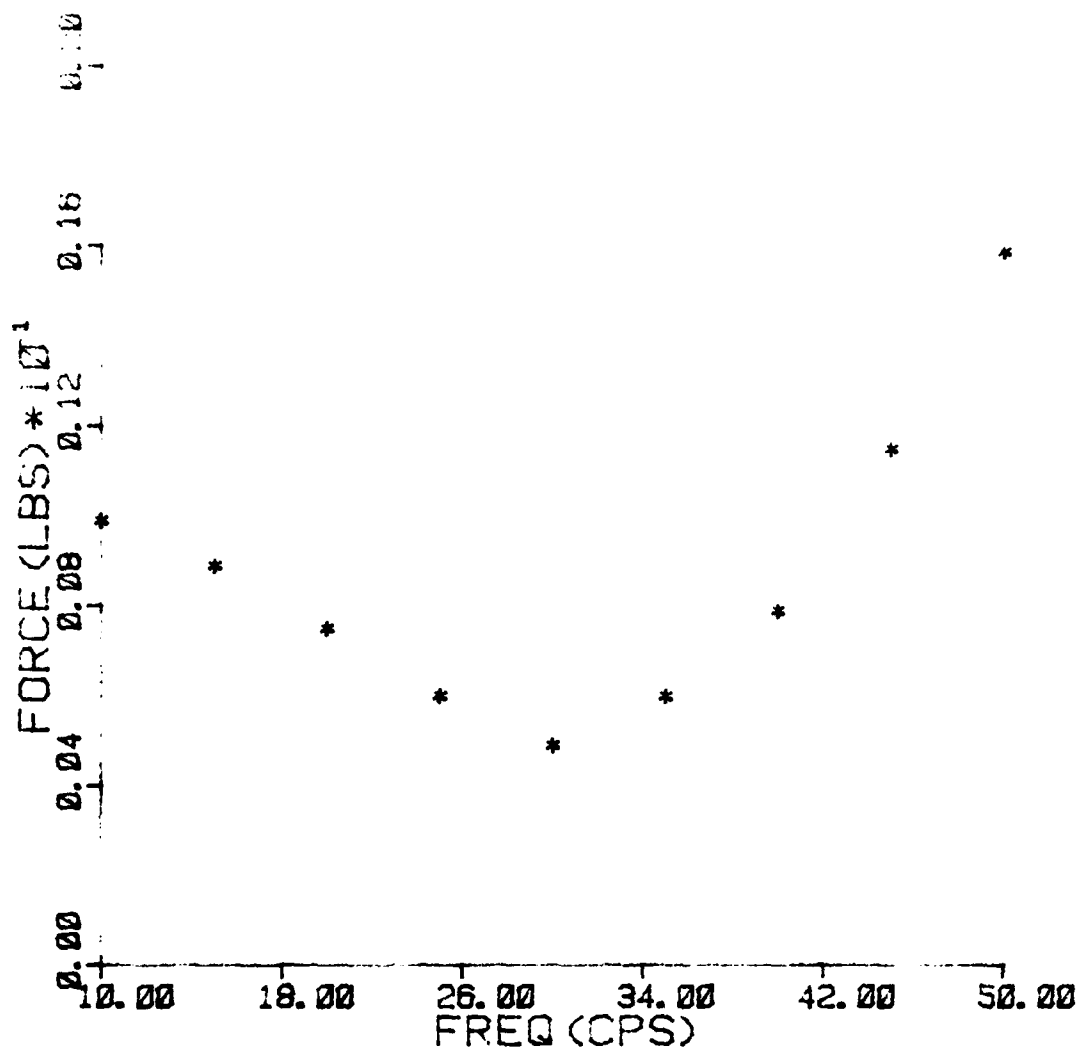
Figure 30 is a plot of  $F_0$  versus  $\omega$  for frequencies between 10 cps and 50 cps. The following values were used in equation 15 when determining the values of  $F_0$ :

$$G_1 = 43 \text{ lb/in}^2$$

$$x = 150 \text{ } \mu \text{ inches}$$

$$\eta = .5$$

$$\omega_n = 31.26 \text{ cps}$$



Analytical Prediction of Force  
Versus Frequency for Rigid Body  
Mode at 150  $\mu$  Inch Displacement  
Figure 30

### VITA

Stephen Lee Vest was born on 10 August 1947 in New Orleans, Louisiana. In 1965 he graduated from high school in New Orleans and enlisted in the U.S. Air Force the following year. He left the Air Force in 1970. In 1976 he graduated from the University of New Orleans with a Bachelor of Science degree in Engineering Sciences. He then reentered the Air Force and completed the Officer Training Program. While assigned to the Air Force Space Division in Los Angeles, California, as a project engineer, he completed a Master of Business Administration Degree at the California State University in Dominguez Hills. He is married to the former Cynthia Faye Bowman and has two children, Lisa and Matthew. In June 1980 he entered the School of Engineering at the Air Force Institute of Technology.

Permanent Address: 6417 Wilburton Drive  
San Diego, Calif 92121



UNCLASSIFIED

SECURITY CLASSIFICATION OF THIS PAGE (When Data Entered)

REPORT DOCUMENTATION PAGE		READ INSTRUCTIONS BEFORE COMPLETING FORM										
1. REPORT NUMBER AFIT/GAE/AA/81D-32	2. GOVT ACCESSION NO. ADA118135	3. RECIPIENT'S CATALOG NUMBER										
4. TITLE (and Subtitle) VISCOELASTIC DAMPING OF TURBINE AND COMPRESSOR BLADE VIBRATIONS		5. TYPE OF REPORT & PERIOD COVERED MS Thesis										
		6. PERFORMING ORG. REPORT NUMBER										
7. AUTHOR(s) STEPHEN L. VEST		8. CONTRACT OR GRANT NUMBER(s)										
9. PERFORMING ORGANIZATION NAME AND ADDRESS Air Force Institute of Technology (AFIT-EN) Wright-Patterson AFB, Ohio 45433		10. PROGRAM ELEMENT, PROJECT, TASK AREA & WORK UNIT NUMBERS										
11. CONTROLLING OFFICE NAME AND ADDRESS		12. REPORT DATE March, 1982										
		13. NUMBER OF PAGES 78										
14. MONITORING AGENCY NAME & ADDRESS (if different from Controlling Office)		15. SECURITY CLASS. (of this report) Unclassified										
		15a. DECLASSIFICATION DOWNGRADING SCHEDULE										
16. DISTRIBUTION STATEMENT (of this Report) Approved for public release; distribution unlimited												
17. DISTRIBUTION STATEMENT (of the abstract entered in Block 20, if different from Report)												
18. SUPPLEMENTARY NOTES <div style="display: flex; justify-content: space-between;"> <div> <p><i>Lynn E. Wolaver</i> LYNN E. WOLAVER Dean for Research and</p> </div> <div> <p><b>APPROVED FOR PUBLIC RELEASE: IAW AFR 190-17</b> AIR FORCE INSTITUTE OF TECHNOLOGY (ATC) WRIGHT-PATTERSON AFB, OH 45433</p> </div> <div> <p>23 JUL 1982</p> </div> </div>												
19. KEY WORDS (Professional Development necessary and identify by block number) <table border="0"> <tr> <td>Vibration damping</td> <td>Friction damping</td> </tr> <tr> <td>Viscoelastic</td> <td>Shear modulus</td> </tr> <tr> <td>Loss factor</td> <td>Turbine blade</td> </tr> <tr> <td>Complex modulus</td> <td>Compressor blade</td> </tr> <tr> <td>Cantilever beam</td> <td>Eigenvalue</td> </tr> </table>			Vibration damping	Friction damping	Viscoelastic	Shear modulus	Loss factor	Turbine blade	Complex modulus	Compressor blade	Cantilever beam	Eigenvalue
Vibration damping	Friction damping											
Viscoelastic	Shear modulus											
Loss factor	Turbine blade											
Complex modulus	Compressor blade											
Cantilever beam	Eigenvalue											
20. ABSTRACT (Continue on reverse side if necessary and identify by block number) An experimental and an analytical model of a turbine/compressor blade is developed in order to investigate the feasibility of using a viscoelastic material to damper the vibrations of the blade. The experimentally determined response of the blade at various frequencies is studied. In order to make a qualitative comparison of damping effectiveness, the response of a similar model using friction damping is also experimentally studied. A model of a modified cantilever beam is used to develop the equation of motion of the												

DD FORM 1 JAN 73 1473

EDITION OF 1 NOV 65 IS OBSOLETE


UNCLASSIFIED

SECURITY CLASSIFICATION OF THIS PAGE (When Data Entered)

UNCLASSIFIED

SECURITY CLASSIFICATION OF THIS PAGE (When Data Entered)

Y blade and the resulting eigenvalue problem is solved using an iterative technique. An analysis of the rigid body mode is performed. A comparison and an analysis of the results of the experimental and analytical models are delineated.



UNCLASSIFIED

SECURITY CLASSIFICATION OF THIS PAGE (When Data Entered)

**DATE**  
**FILME**